Review

Composition and Basic Physical Properties of the Phobos Surface: A Comprehensive Review

Malwina Kolano * , **Marek Cała** and **Agnieszka Stopkowicz**

Faculty of Civil Engineering and Resource Management, AGH University of Krakow, 30-059 Krakow, Poland; cala@agh.edu.pl (M.C.); agnieszka.stopkowicz@agh.edu.pl (A.S.)
* Correspondence: mkolano@agh.edu.pl

Abstract: The surface of Phobos is an intriguing subject of research for many scientists. This is associated, among other things, with the fact that it is perceived as a potential launch site for future human Mars exploration. Additionally, measurements conducted on its surface would not only deepen our knowledge about Phobos but also provide insights into geochemical processes occurring on similar small bodies in the Solar System. Therefore, understanding the physical–mechanical properties of regolith is a crucial aspect of planetary exploration. These properties are key factors needed for both planning safe landings and establishing future bases on celestial bodies. In this paper, information is compiled regarding hypotheses about its origin, the probable composition of Phobos' surface (spectral properties and HiRISE data), as well as its morphology. The article also presents the process of regolith formation covering Phobos' surface and its presumed physical properties. It has been established that the estimated bulk density of Phobos, compared to the densities of other asteroids and meteorites, is most similar to C-type asteroids. It was also found that C-type asteroids, in terms of total porosity, best reflect Phobos. However, determining the surface composition of Phobos and its detailed physical properties requires additional information, which could be obtained through in situ studies or sample return missions.

Keywords: Phobos; composition of the surface; morphology; regolith; physical properties

1. Introduction

Phobos is one of the two moons of Mars. It was discovered in 1877 by Asaph Hall, an astronomer from the United States Naval Observatory. It moves deep within Mars' gravitational field [1,2]. Its first close approaches were made by the Mariner 9 spacecraft in 1971. Many imaging data come from the Viking 1 and Viking 2 orbiters (data acquired in the late 1970s). Based on these data, the first shapes were interpreted, and dynamic models of Phobos were created. Close observations of Phobos were also made by the spacecraft Phobos 2 (100 km from landing on Phobos, 1988), Mars Global Surveyor (1996–2006), and Mars Reconnaissance Orbiter (since 2005). Currently, the only spacecraft that regularly encounters Phobos and provides extensive data about this satellite is Mars Express [3].

Since its discovery, Phobos has garnered significant interest from astronomers and researchers, and its origin remains an open question. Scientists planning space missions have identified Phobos as a target for research, from which acquiring extraterrestrial samples might be "relatively" straightforward. Additionally, Phobos is perceived as a potential launch site for future human Mars exploration. It has been suggested that Phobos could serve as a "pit stop" for crewed Martian missions [2,4]. Furthermore, measurements conducted during operations near Phobos and potential landings on its surface could fill gaps in the knowledge required for the exploration of Mars' moons. Using a penetrator, or other devices on its surface related to determining the mechanical properties of the material, would aid in understanding the geotechnical properties of regolith. A brought-back sample could help to determine the availability of resources as well as the mineral, elemental, and

isotopic composition of the regolith. It would also provide a better characterization of the effects of cosmic weathering in the Martian environment. Additionally, the shape and volume could be much more accurately determined than they currently are [4].

2. Phobos

Phobos is a small and irregularly shaped celestial body (Figure 1) with dimensions of 13.0 × 11.4 × 9.1 km [5,6], a volume of 5742 ± 32 km^3 [7], and a gravitational mass of GM = 7.11 ± 0.09 × 10^{-4} km^3·s^{-2} (GM determined along with the uncertainty range, considering most solutions from flybys, gravitational field extractions, and "distant" encounters) [8].

Figure 1. Phobos from 6800 Kilometers (Color). Image taken by the High Resolution Imaging Science Experiment (HiRISE) camera on NASA's Mars Reconnaissance spacecraft [9].

Asteroids are divided into different spectral types, including asteroids of C, D, and T types, with the following definitions:

- C-type asteroids—a very dark and non-reflective type of asteroid, gray in color, with a composition believed to be similar to that of carbonaceous chondrites.
- D-type asteroids—a very dark and non-reflective asteroid, reddish in color, probably due to the surface presence of organic materials.
- T-type asteroids—a rare type of asteroid with a fairly low albedo and a moderate absorption feature at wavelengths shorter than 0.85 micron.

The surface of Phobos is very dark, with an albedo not exceeding a few percent, and its spectra are similar to the spectra of D-type asteroids, which are often found in the outer main asteroid belt and the outer Solar System [10].

The gravitational field of Phobos is small due to its small size and is highly non-uniform due to its irregular shape (g = 5.7×10^{-3} ms^{-2}, [11]). Consequently, the escape velocity from Phobos' surface is highly variable [12] and ranges from ~4 to 10 ms^{-1} (depending on the latitude and longitude, as well as the local time of the launch site on Phobos) [13].

The orbit of Phobos is nearly circular and almost equatorial, with a distance to the center of Mars of approximately 2.76 R_M, where R_M represents the radius of Mars (3396 km) [1,14] Additionally, the orbit gradually decays as it approaches Mars due to the tidal forces dissipated within the planet. Consequently, in approximately tens of millions of years, Phobos will be torn apart by tidal forces and disintegrate in the Martian atmosphere [14].

The general orbit data are summarized in Table 1.

Table 1. The general orbit data of Phobos [14,15].

Semi-Major Axis	Eccentricity	Inclination to the Equator	Orbital Period
9375 km (2.76 R_M)	0.0151	1.076°	7 h 39′ 19.47″

3. Hypotheses of Formation

3.1. Capture Hypothesis

The capture hypothesis posits that Phobos is a "captured" asteroid. The main arguments supporting the capture scenario are the morphological, physical, and spectroscopic similarities between the moon of Mars and primitive asteroids [14,16]. The resemblance between the surface spectra of the Martian moon and D- or T-type asteroids suggests that the moon is composed of the same material as these asteroids, namely, carbonaceous material [1]. This scenario would explain its low density and low albedo.

Several possible scenarios have been proposed that would be consistent with the capture hypothesis and the current orbit. The first suggests that the body was captured into an equatorial orbit. However, maintaining an orbit in the equatorial plane would require a rapid change in the distance between the orbit and Mars (approximately 13R_M, where R_M is the average radius of Mars, equal to ~3396 km) shortly after its capture, which seems challenging given how slowly the orbit eccentricity is modified by tidal effects [1,14,17]. The second solution posits that the orbit, after the body's capture, was quickly inclined in the equatorial plane and rounded by the scattering of resistance in the planetary nebula [18,19]. However, studies of the resistance effect have not yet shown whether the density profile and the lifetime of the nebula are consistent with the requirements of the capture scenario [14].

It should be noted that if the Martian moons (Deimos and Phobos) were indeed captured, either they shared the same original composition (originating from the same body) or they underwent extensive cosmic weathering, resulting in the formation of nearly identical surfaces [4].

However, the capture hypothesis is considered less likely due to the fact that dynamic capture models require specific conditions, including aerodynamic drag in the early proto-atmosphere of Mars [4,10,18,20]. Additionally, the nearly equatorial and nearly circular orbit of Phobos is considered unlikely for this scenario [1,10,14,17]. Furthermore, such a scenario would require the consideration of a mechanism that would change the orbit of the Martian satellite post-capture to the one currently observed. One possible mechanism for achieving this is the dissipation of orbital tides [14,21]. However, this mechanism would not be sufficient for Deimos (Mars' second moon) [14,22]. Additionally, the orbital changes induced by tides require a very low tidal quality factor, more suitable for icy material than for rocky material [1].

3.2. In Situ Formation Hypothesis

The challenges in reconciling the capture hypothesis with the current orbital properties of Mars' moons motivate the exploration of alternative hypotheses. One such hypothesis proposes that the moons of Mars originated from an equatorial disk of remnants containing material beyond the Martian realm. This alternative hypothesis suggests that the Martian moons formed from an equatorial disk of debris, which also included matter beyond the Martian vicinity [23].

In this hypothesis, the parameters most challenging to explain in capture scenarios (orbital eccentricity and inclination) are considered natural outcomes of the accretion of the circumplanetary disk [1,14,24]. Additionally, if Phobos originated from loosely aggregated material from the accretion disk, its small mass (low bulk density) would be easily explainable, implying likely high porosity [1,14,25]. These characteristics would account for the formation of major morphological features on Phobos' surface, such as the Stickney crater [14,26] and some of its grooves [14,27].

There are two main scenarios for in situ formation. One of them posits that a body significantly more massive than Phobos was captured by Mars; subsequently, its orbit rapidly decayed due to tidal forces, and the object was destroyed upon crossing the Roche limit [28]. From the resulting debris below the Roche limit, a ring formed around Mars, giving rise to small moons. However, the Roche limit is approximately $3R_M$, well below the synchronous limit, which is around $6R_M$. It is challenging to identify a mechanism by which moons formed near the Roche limit could migrate far from Mars and then remain in orbit for an extended period [14,29].

Another possibility is the formation of Phobos resulting from a giant impact [1,24]. The scenario of the Martian moons forming due to a giant impact is one of the more recent hypotheses. Craddock's research [30] suggests that a large body (from one-quarter to one-third the size of Mars) collided with proto-Mars at least 4 billion years ago, ejecting fragmented material into space. Simulations by Citron et al. [31] indicate that impacts forming basins the size of Borealis could eject a sufficient amount of material, creating an accretion disk from which the Martian satellites formed (accretion in the strong tidal regime hypothesis).

The key factor in this formation scenario is the rotation imparted to the planet by the impactor because it determines the location of the synchronous boundary (whether it is within or beyond the Roche limit). A slow rotator, like Mars post-impact, corresponds to a relatively distant synchronous boundary. Moons that form near the Roche limit, due to the viscous spreading of the disk, migrate outward through interactions with the remaining disk but eventually settle back towards Mars under the influence of tidal forces. It is expected that only small moons formed near or beyond the synchronous boundary will remain in orbit for an extended period [14]. Phobos and Deimos may be the last surviving moons that emerged from the formed accretion disk (Figure 2). The current rotation of Mars suggests a relatively massive impactor, which could also be responsible for the formation of the Borealis basin [32].

The giant impact scenario is also consistent with telescopic observations of the surfaces of both moons, suggesting a composition different from that of Mars. In this case, the composition of the disk materials is treated as a mixture of Martian and impactor materials (Figure 3) [14].

Numerical simulations used to replicate the entire scenario of Phobos' formation, from the initial impact to accretion and the long-term evolution of the two moons, provide better agreement with their current orbits than the previous capture hypothesis and remain consistent with observations regarding their composition [14].
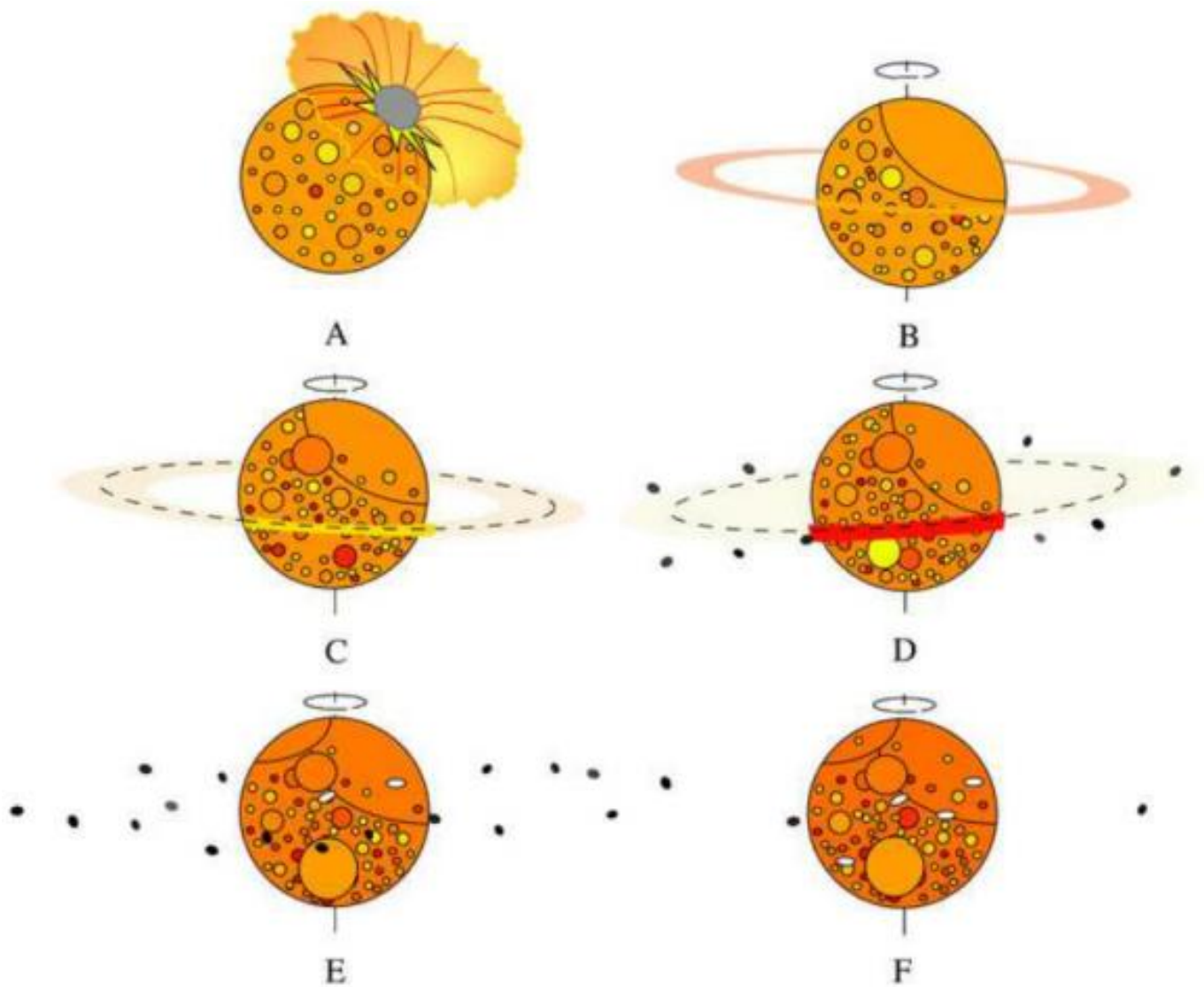
Figure 2. Schematic of the formation of Phobos and Deimos—giant impact scenario. (**A**) A large body (from one-quarter to one-third the size of Mars) (impactor) collides with proto-Mars (rotator), ejecting fragmented material into space; (**B**) the ejected material forms an accretion disk; (**C**) Materials disperse beyond the Roche limit (dashed line) and begin to coalesce into small moons; (**D**) moons form until the accretion disk is exhausted (Deimos forms beyond synchronous rotation); (**E**) the accretion disk is entirely depleted, and dozens of small moons orbit Mars. Tidal perturbations cause these moons to fall back onto the surface of Mars (white ellipses); (**F**) the present Martian system with Phobos and Deimos in orbit [14,30].
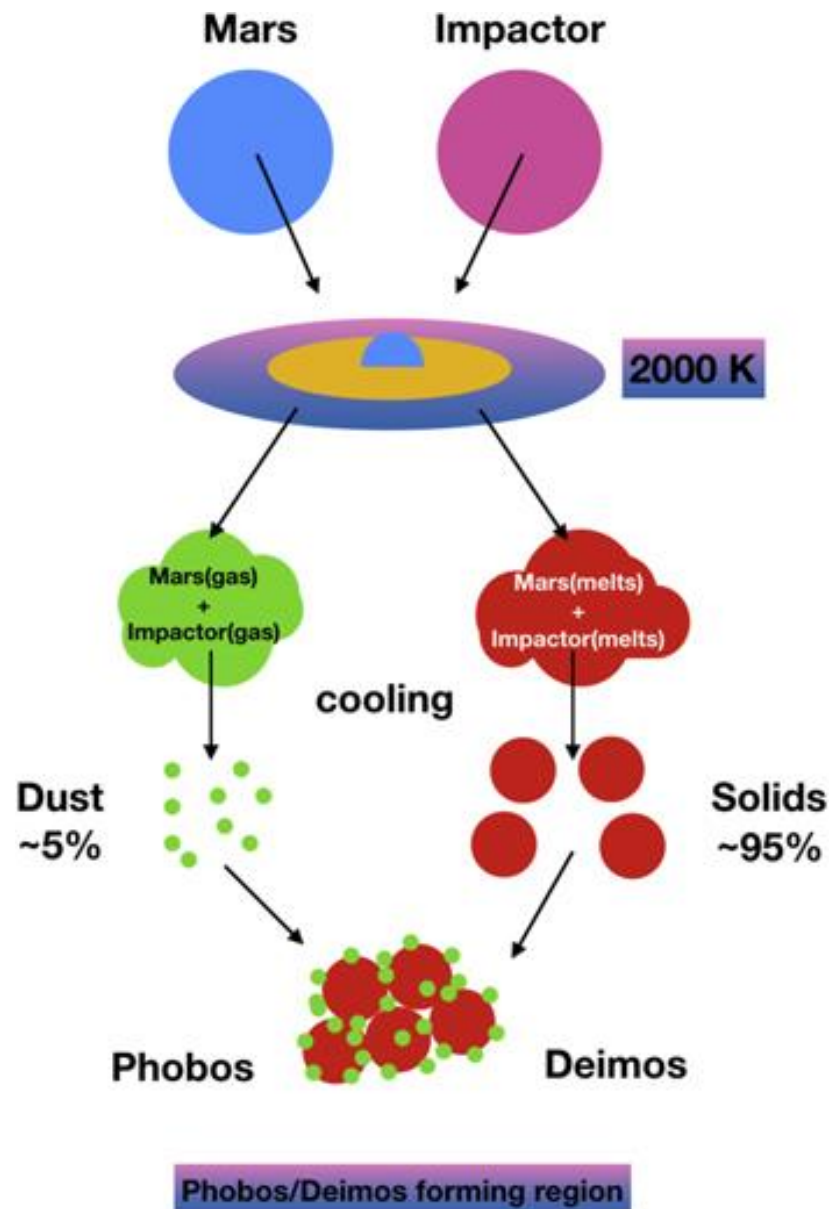
Figure 3. Schematic representation of chemical modeling; the scenario of a giant impact [33] (the yellow region represents the part of the disk within the Roche limit [34]).

4. Surface Composition of Phobos

4.1. Spectral Properties

Visible spectra obtained through spectrometer imaging in the near-infrared range are commonly employed for the identification or, at the very least, constraint of the surface mineralogy of Solar System bodies by identifying highly diagnostic absorption bands of minerals [35]. Available spectroscopic data indicate the presence of two distinct materials on Phobos' surface. Data from Mars Express and Mars Reconnaissance Orbiter have provided additional information regarding the properties of these materials and their spatial relationship.

The surface of Phobos reveals areas with different spectral slopes, defined as red and blue units. The red unit covers the majority of the moon's surface and is characterized by a low albedo and a red spectral slope. The blue unit becomes apparent near the Stickney crater (Figure 4) and exhibits spectral properties similar to the prevalent red unit but with a smaller spectral slope [10].
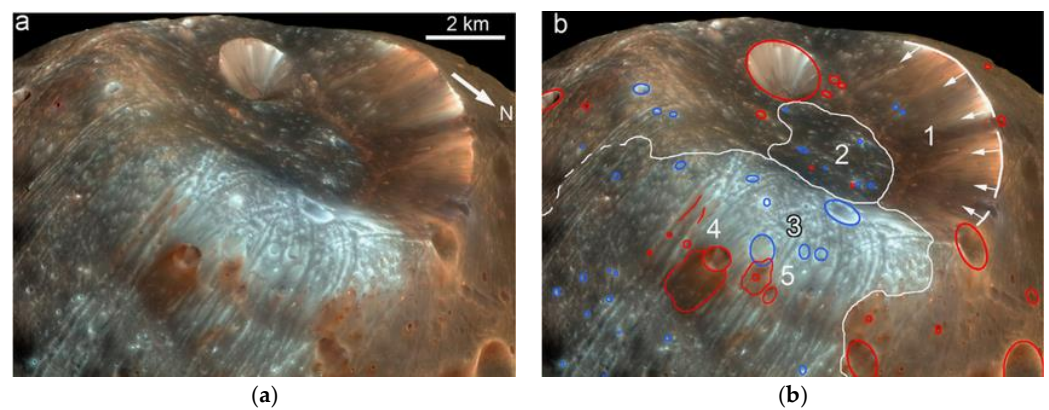
(**a**)   (**b**)

Figure 4. (**a**) View of Stickney crater and its eastern rim; (**b**) the same view with key geological features highlighted. Craters containing red and blue materials are outlined in red and blue, respectively. Red lines indicate outcrops of reddish material along the edges of grooves. White lines show the boundaries of geological units. HiRISE_PSP_007769_9010_IRB image synthesized from photos taken in the infrared (800–1000 nm), red (550–850 nm), and blue-green (400–600 nm) channels [12] (numbers from 1 to 5 according to [12]). Numbers: 1 (and white arrows)—part of the massive landslide moving down from the W-NW sector of the crater inner walls; 2—the hummocky surface texture deposit; 3—the landslide body acquired sufficient momentum for the frontal part of the moving landslide mass to travel up the interior of the wall and onto the eastern rim of the crater; 4—the 700 m crater, whose interior, eastern rim, and the area further to the east are red, while the area around the crater is blue, except the part to the east; 5—crater about 100 m in diameter is surrounded by a relatively wide (200–500 m) red halo, interpreted as its ejecta [12].

The spectra of Phobos' surface reflectance in the near-infrared and visible wavelengths (approximately 0.4 to 4.0 μm) show an increasing slope towards the infrared region, matching several low-albedo primitive asteroids [14]. Phobos' reflectance spectra have been confirmed by missions such as Mars Reconnaissance Orbiter, Mars Express, and Rosetta, as well as observations obtained using the Hubble Space Telescope and the ground-based 4 m Mayall Telescope [14].

So far, no satisfactory spectral match has been found between Phobos and meteoritic material considered representative of primitive asteroids. Additionally, the reflectance spectra do not clearly show absorption bands (Figure 5), which provide diagnostic information regarding the composition of carbonaceous, silicate, or hydrated material. This may be related to cosmic weathering, which can suppress such bands on airless bodies [14]. On the Moon, this process is responsible for darkening, reddening, and damping absorption bands in the reflectance spectra of silicate material [35]. The darkening, reddening, and damping of absorption bands have also been observed in the spectra of Phobos (Figure 5).
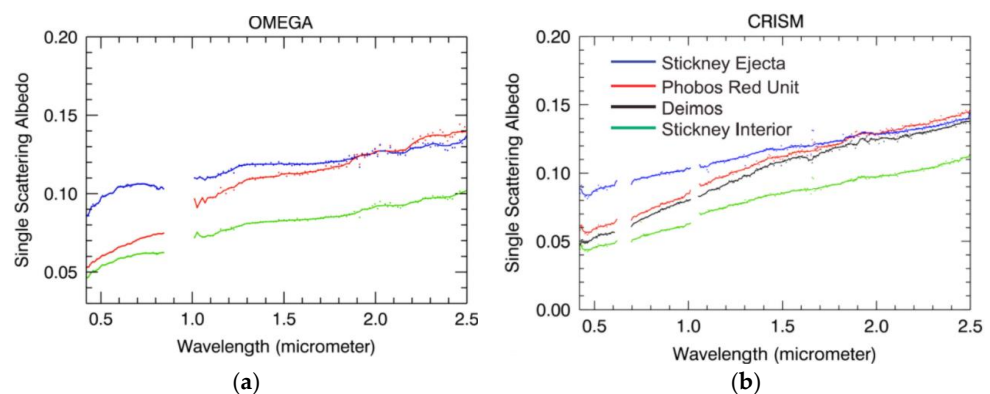

(**a**)   (**b**)

Figure 5. Reflectance spectra obtained by instruments: (**a**) CRISM from Mars Express; (**b**) OMEGA Mars Reconnaissance Orbiter [36].

In the spectra of Phobos, an uncertain and very weak absorption band around 0.65 μm has been detected (Figure 6), which can be interpreted as a potential signature of composition. However, the possibility of cosmic weathering effects cannot be ruled out [37]. The interaction with carbonaceous material is less understood than with silicate material and may lead to the development of red or even blue spectral slopes observed in the reflectance spectra of carbonaceous asteroid surfaces [14,38]. The impact of cosmic weathering on reflectance spectra has been preliminarily simulated for carbonaceous meteorite samples, but the results showed limited resemblance to the spectra of Phobos and Deimos [14,39].
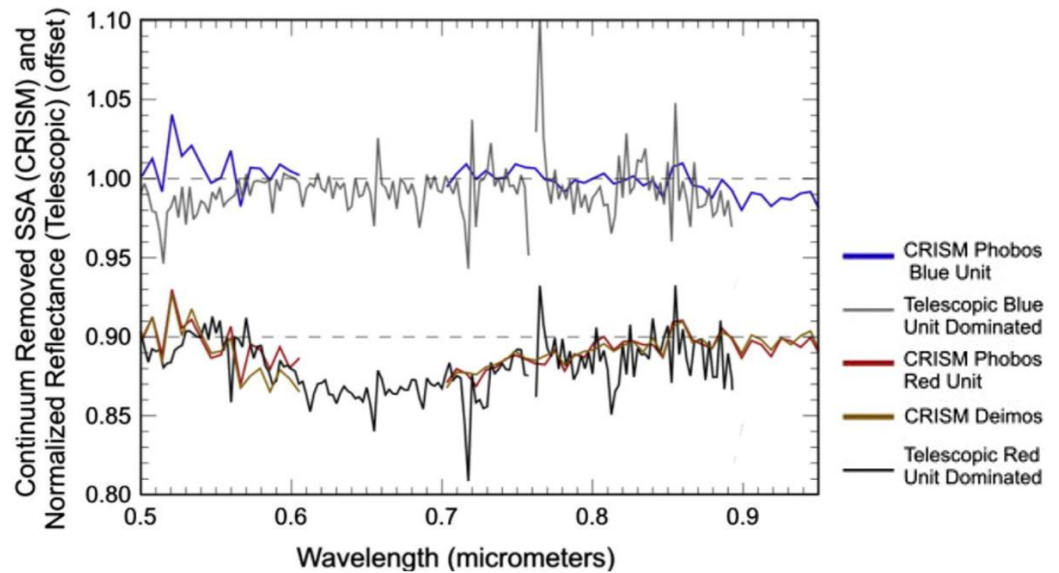

Figure 6. CRISM and telescope observations—approximate small absorption band at around 0.65 μm for Deimos and for the red unit of Phobos [37].

Emissivity spectra (wavelengths ranging from 5 to 50 μm), in contrast to reflectance spectra, exhibit distinct features more typical of silicates than of carbonaceous meteorites (Figure 7) [40]. However, they have lower spatial resolution compared to reflectance spectra and are also more susceptible to the grain sizes of surface regolith and, to some extent, cosmic weathering [14,35].
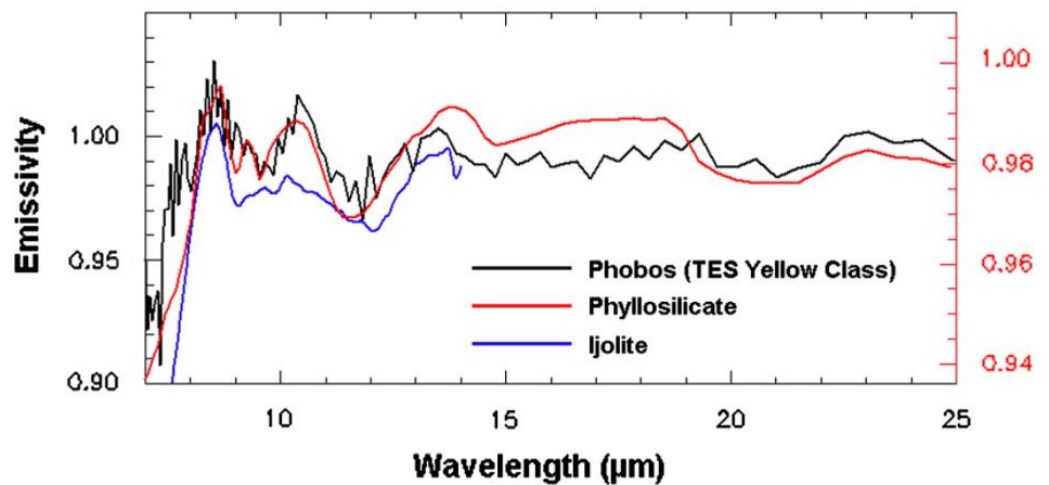

Figure 7. Matching the emissivity spectrum (thermal radiation emission) of Phobos' surface with spectra of silicate material (vertical color-coded curves correspond to the right axis) [40].

Determining the actual composition of Phobos' surface based solely on spectroscopic observations may not be feasible. Reflectance spectra suggest the presence of carbonaceous

material [37], while emissivity spectra indicate the presence of silicates [40]. Recently, a hypothesis has been proposed that dark regions (anorthositic) on the Moon may have low albedo similar to those on Phobos [41].

It is important to note that spectral observations of moons are obtained under various lighting conditions, making their comparison with spectra of well-characterized laboratory samples collected under controlled lighting conditions challenging [37].

4.2. High-Resolution Imaging (HiRISE)

Details regarding the two types of materials detected on Phobos were further examined using enhanced-color images from HiRISE (High-Resolution Imaging Science Experiment) (Figure 8).
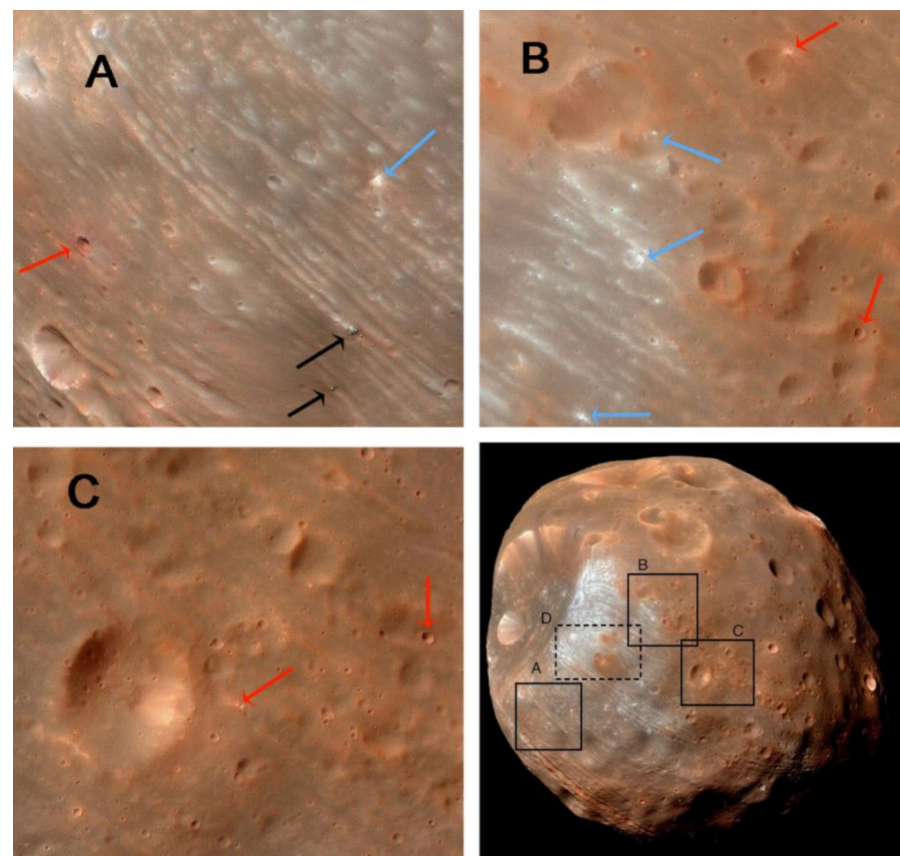

Figure 8. (**A**–**C**) HiRISE PSP_007769_9010_IRB—"red" and "blue" surface units (red and blue arrows—craters located, respectively, in the "red" and "blue" unit; black arrows—exposed rocks). Subsection D illustrating relations between materials along the rim of Stickney [35].

Despite the high detail of the images, neither a straightforward spatial distribution nor a stratigraphic relationship between the "red" and "blue" materials was observed. Some boundaries between them appear relatively well-defined (Figure 8B), while others are blurry (Figure 8A). The red material dominates within craters of all sizes (Figure 8C), except for the eastern rim of the Stickney crater. There is also no apparent color–age relationship; fresh (recent) craters expose both types of materials in various locations (red and blue arrows in Figure 8) [35].

Considering the observed spatial relationships, it is challenging to formulate a single model in which the red unit is predominantly depositional or originates from the blue unit due to cosmic weathering [35]. The preferred model for Phobos, consistent with the currently available observational data, suggests that it is primarily a heterogeneous object composed of a mixture of red and blue material blocks of varying sizes (Figure 9) [12].
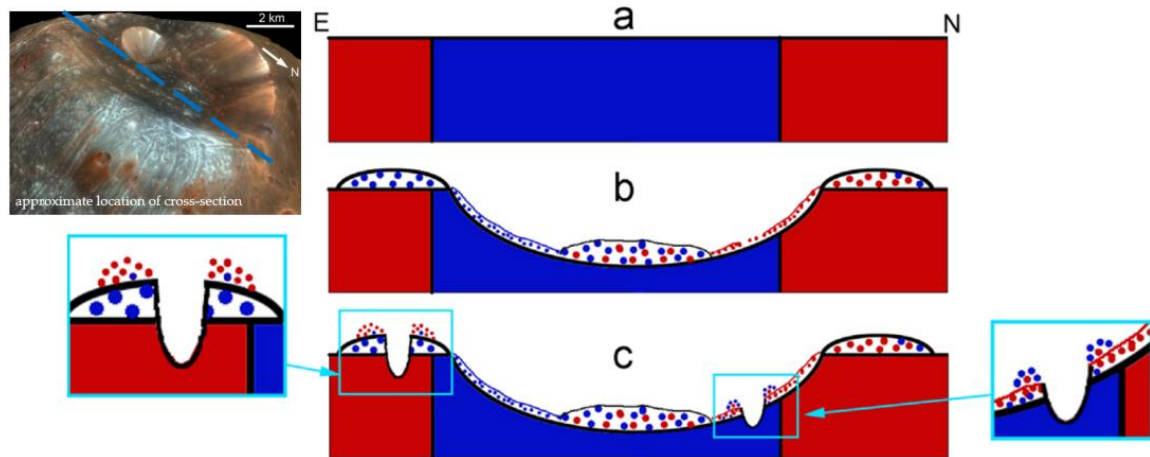
Figure 9. A schematic cross-section through the Stickney crater (from its eastern rim towards its center to its northern rim) with delineated stages of the formation of the observed morphology and distribution of red and blue units: (**a**) stage 1, (**b**) stage 2, and (**c**) stage 3 [12].

It is worth emphasizing here that even if the above model is correct, the composition of these two components and how the material was mixed and transformed remain unknown [35].

4.3. Speculative Composition of Phobos

4.3.1. Capture Hypothesis

If Phobos is a captured asteroid, then the majority of its mass may consist of primitive carbonaceous material, possibly akin to D-type bodies from the outer asteroid belt. Generally, D-type asteroids are believed to contain volatile components; however, these asteroids, significantly distant from the Sun, typically do not exhibit features of molecular water absorption, leading to the possibility that their composition might be anhydrous silicates [4]. In Phobos spectra, no definitive evidence of features indicating molecular water absorption has been detected (e.g., [10,36,37]). It is conjectured that the high daytime surface temperature of Phobos and the presence of fragmented, weathered regolith may have desiccated hydrated minerals to depths of several centimeters or more [4].

Murchie et al. [4], based on various models of Phobos' origin, proposed its composition, drawing parallels to different types of meteorites (Table 2). Depending on the analyzed variant of Phobos' origin, the authors indicated the predicted composition, as well as the composition of elements and minerals. A compilation of this information is presented in Table 2.

Table 2. The predicted composition of Phobos depending on the type of captured body [4].

Origin Hypothesis	Composition Predicted	Elemental Abundance	Mineral Abundances
Capture of organic- and water-rich outer solar system body	Ultra-primitive composition (Tagish Lake is the best known analog)	High C. High Zn/Mn. High S. Composition possibly unique compared to known meteorites.	Abundant phyllosilicates. Carbonates and organic phases. Anhydrous silicate phases rare.
Capture of organic- and water-poor outer solar system body	Anhydrous silicates plus elemental carbon	High C. Mg/Fe ratio ~2–4. Bulk composition unlike any meteorite analogs.	Anhydrous, med. Fe (20–40%) pyroxene + olivine. Abundant amorphous carbon or graphite?
Capture of inner solar system body	Composition like common meteorites (e.g., ordinary chondrites)	Mg/Si ~0.8–1. Al/Si ~0.05–0.1. Zn/Mn and Al/Mn ratios separate known meteorites. Likely low C.	Low carbonates, phyllosilicates. Pyroxene, olivine probably in range of known meteorites.

4.3.2. Giant Impact Hypothesis

If Phobos formed as a result of a giant impact (high-energy collision) capable of creating the Borealis basin [42], it should consist of roughly half Martian material and half impactor material [34]. Interaction with lower energy may result in a higher content of Martian material, up to 80% [14,43]. However, the final composition should be quite similar to that predicted by Pignatale et al. [33], but with less iron-rich silicate dust [14]. Additionally, it is hypothesized that the Martian material will largely originate from the Martian mantle (depths up to ~50–150 km) [34].

If the giant impact hypothesis is correct, Phobos should be depleted in volatile substances such as water vapor because impacts are generally energetic events [32,34].

Pignatale et al. [33], in investigating the chemical composition of the building blocks of Phobos (and Deimos) in the giant impact scenario, utilized thermodynamic equilibrium calculations. A schematic of this chemical modeling in the giant impact scenario, where dust originates from condensing gas and solid bodies form from solidifying material, is presented in Figure 3.

Thermodynamic calculations, utilizing various types of impactors (such as Mars, carbonaceous chondrites, enstatite chondrites, and comets), predict a wide variety of final compositions carrying different amounts of C, H, O, Fe, and Si [33].

Each type of impactor should impart specific, unique markers [33], for example, the following:

- Mars + CV (CV—carbonaceous chondrites) would contain large amounts of metallic iron, SiO_2, iron sulfides, and carbon;
- Mars + Comet would have pyroxenes and the highest content of carbon and ice;
- Mars + EH (EH—enstatite chondrites) would contain a high content of metallic iron, SiO_2, iron sulfides (FeS and MgS), and trace amounts of SiC;
- Collisions with Mars-like objects would yield iron oxides;
- Mars + CI (CI—carbonaceous chondrites) would include iron oxides, water ice, and carbon.

The presence or absence of compounds such as metallic iron, iron oxides, iron-rich silicates, sulfides, carbon, or water ice could indicate the nature of the impactor [33].

5. Surface Morphology of Phobos

5.1. Craters

On the surface of Phobos, there are 1300 craters with a diameter greater than 200 m. Among them, 70 craters have a diameter greater than 1 km, and 26 have a diameter greater than 2 km [12]. Seventeen craters have been officially named [44]. The largest crater is Stickney, with a diameter of approximately 8 km (Figure 10) [12] (other researchers provide slightly different dimensions, approximately ~11 km—[45]; ~10 km—[1]; ~9.5 km—[46]). Comparisons between the surface of Phobos and the Moon suggest that craters with diameters in the decimeter and centimeter range should also be present, and impact microcraters should be found on the surfaces of rock fragments.

Despite Phobos being a very small celestial body, it is covered with craters that resemble those found on larger planets. Craters with diameters of 100–200 m or smaller are very similar in size and shape to craters on the Moon [47].

Most craters are of impact origin, although some small craters may be features formed by the penetration of regolith into subsurface fractures [12,46].

Most of the craters on Phobos have a bowl-shaped morphology (Figure 11), while some display complex internal features (approximately 60 craters). Three types of craters with complex morphology can be distinguished: flat-floored craters, craters with a central mound, and concentric craters (Figure 12). Among craters with complex internal morphology, concentric craters are the most common, while craters with a flat floor and a central mound are relatively rare [12].
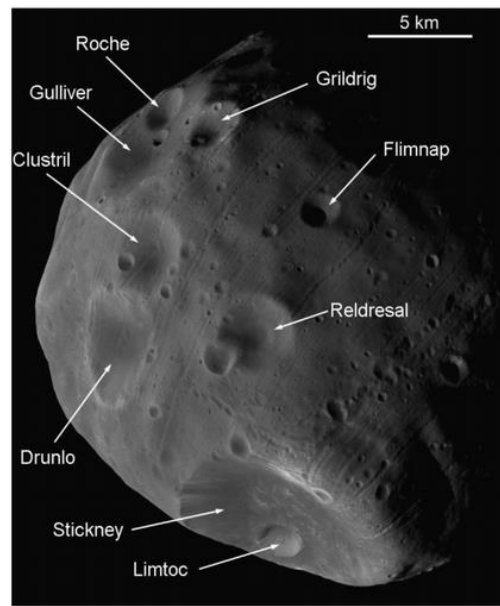
Figure 10. The HRSC (High-Resolution Stereo Camera) image h0756 depicts craters and grooves [12].
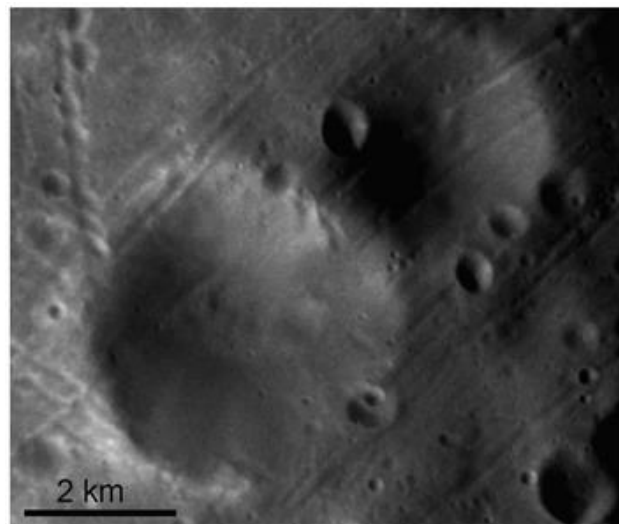

Figure 11. A fragment of the HRSC (High-Resolution Stereo Camera) image h2780 shows the crater Drunlo (bottom left corner, diameter 4.2 km) and the crater Clustril (top right corner, 3.4 km) [12].
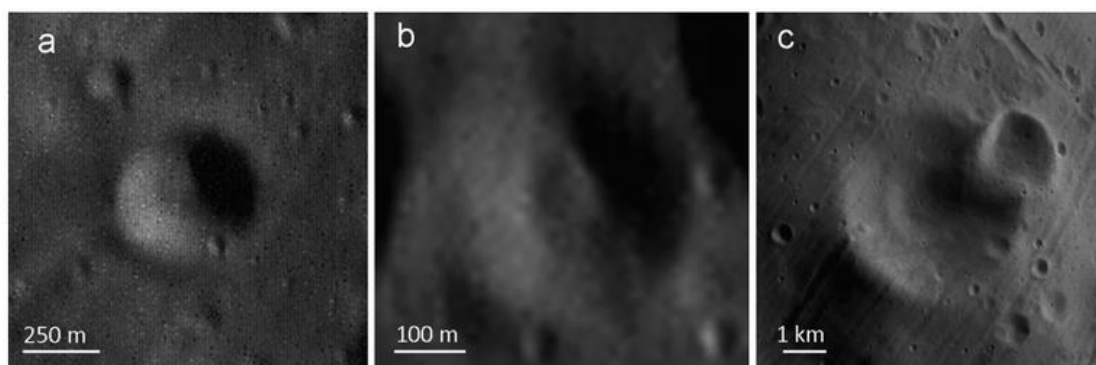

Figure 12. Portions of HRSC image h0756: (**a**) flat-floored crater (diameter 480 m), (**b**) crater with a central mound (diameter 350 m), and (**c**) concentric crater Reldresal (diameter 2.9 km) [12].

Craters with a diameter greater than 200 m also exhibit external morphological variability (Figure 13). A relatively small number of craters have an elliptical shape (Figure 13a). Some craters feature polygonal planimetric outlines, such as the square-shaped Hall crater (Figure 13b). This crater has two opposite linear edges coinciding with the undulating surface features of the substrate and two opposite linear edges approximately perpendicular to the previous ones, parallel to the system of grooves. The planimetric outlines of the 4.6 km long Drunlo crater (Figure 13c) show a certain triangular shape, with two directions coinciding with the groove systems [12].
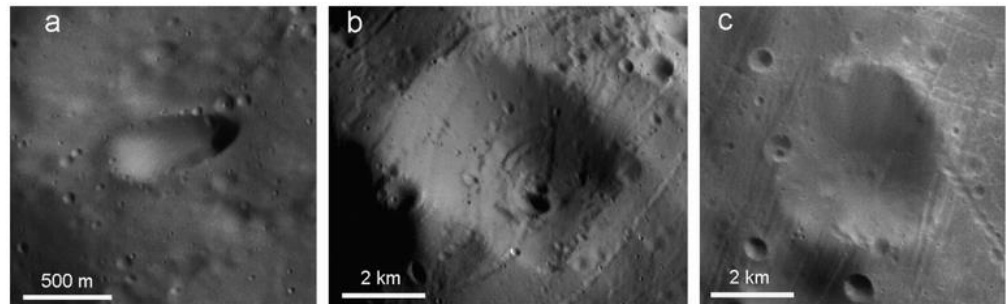

Figure 13. Portions of HRSC images h8974, h9574, and h2780: (**a**) elliptical crater with lengths of 750 m and 250 m, (**b**) Hall crater with a diameter of 6.2 km, and (**c**) Drunlo crater with a length of 4.6 km [12].

Utilizing the digital terrain models (DTMs) of Phobos, Basilevsky et al. [12] classified craters with a diameter greater than 2 km into three morphological classes based on the ratio of d/D (depth to diameter) and the maximum slope/steepness of the inner walls (Figure 14). The following classes were distinguished [12]:

- Class 1—d/D > 0.1, maximum slope of inner walls > 20° (may rich 40–50°);
- Class 2—0.05 < d/D < 0.1, maximum steepness of inner walls 10–20°;
- Class 3—d/D < 0.05, maximum steepness of inner walls 10°.

According to this classification, 38% of Phobos' craters belong to class 1, 29% to class 2, and 33% to class 3. This subpopulation of Phobos' craters (craters with a diameter greater than 2 km) has a significantly higher number of craters with gentle slopes compared to craters on the Moon. This may be due, in part, to Phobos' very low gravity [12].
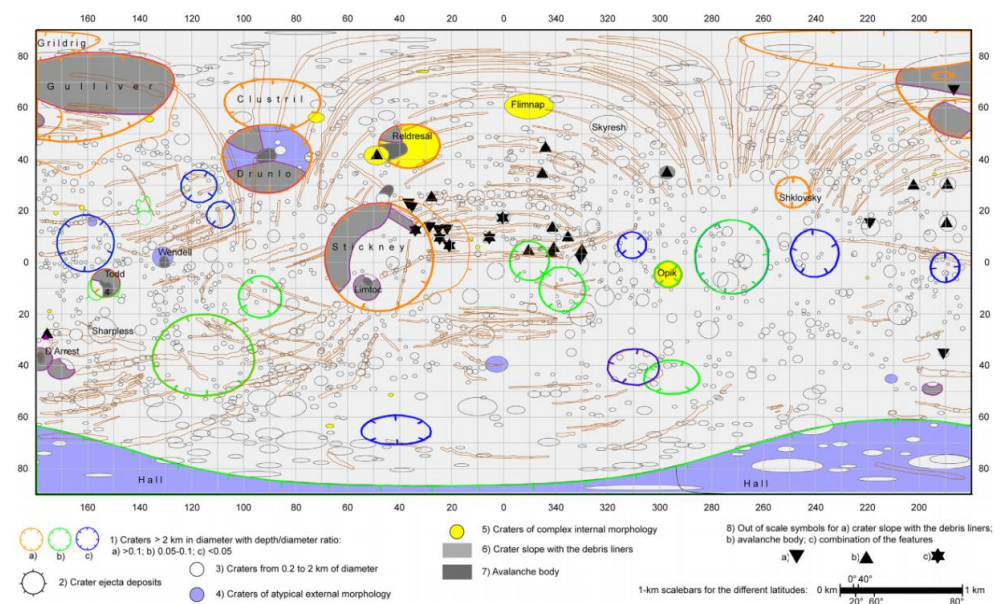

Figure 14. Geomorphic map of Phobos [12].

It is believed that the crater population on Phobos is close to equilibrium, a state in which a further increase in crater density is impossible because each time a new crater forms, a previously formed one is destroyed [12]. The density of craters with a diameter of 41 km is close to the limit of their occurrence. This means that an increase in the density of such craters by one-third would destroy the entire body [12].

5.2. Grooves

Another type of morphological feature characterizing the surface of Phobos is the numerous grooves (Figures 14 and 15) [1,12,48–50].
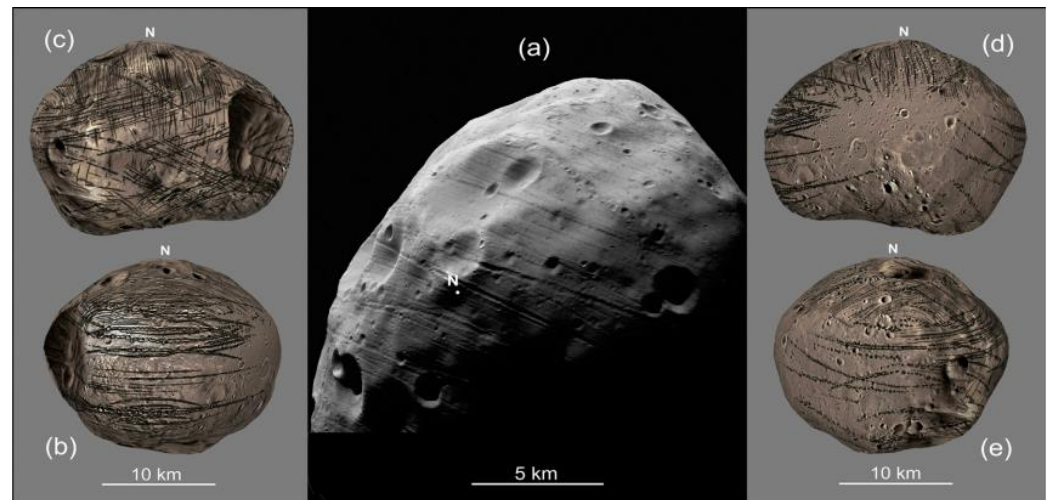

Figure 15. Phobos (**a**) view of the northern hemisphere (Mars Express HRSC Image 401-20080729-5851-6-na-1b, orbit 5851), (**b**) sub-Martian hemisphere, (**c**) leading orbital hemisphere, (**d**) trailing orbital hemisphere, and (**e**) anti-Martian hemisphere [51].

The origin of Phobos' grooves has been a subject of discussion since their discovery. Most likely, the grooves are fractures appearing on the surface of Phobos during strong impacts. Three different mechanisms for the formation of grooves are considered [12,46,49,50]:

- Cracks/faults formed by the shockwave, due to tidal forces and resistance forces during capture;
- Chains of secondary impact craters or ejecta from Stickney (traces of rolling and bouncing boulders);
- Chains of secondary impact craters formed due to large primary impacts on Mars (chains of craters formed by ejecta from large impact craters on Mars).

Presently, it is believed that the grooves on Phobos result from a combination of processes such as impact-induced fracturing with low-velocity ejections, the re-accumulation of ejecta, and tidal stresses [52].

Phobos' grooves are elongated, linear, or nearly linear depressions, typically with a width of 100–200 m and a depth of 10–30 m. Their length usually ranges from a few kilometers, but some may extend up to about 20 km [12,46,53]. At least one groove can be traced continuously for 168°, approximately 30 km [49]. Grooves exhibit variations in appearance. Chain-like groove formations have been identified, formed by connecting depressions/craters of roughly the same diameter. Grooves with serrated edges and almost linear groove formations have also been observed.

Figure 16 illustrates the morphological variations in grooves and the relationships between the grooves and the craters Drunlo (D = 4.2 km) and Clustril (D = 3.4 km) [12].
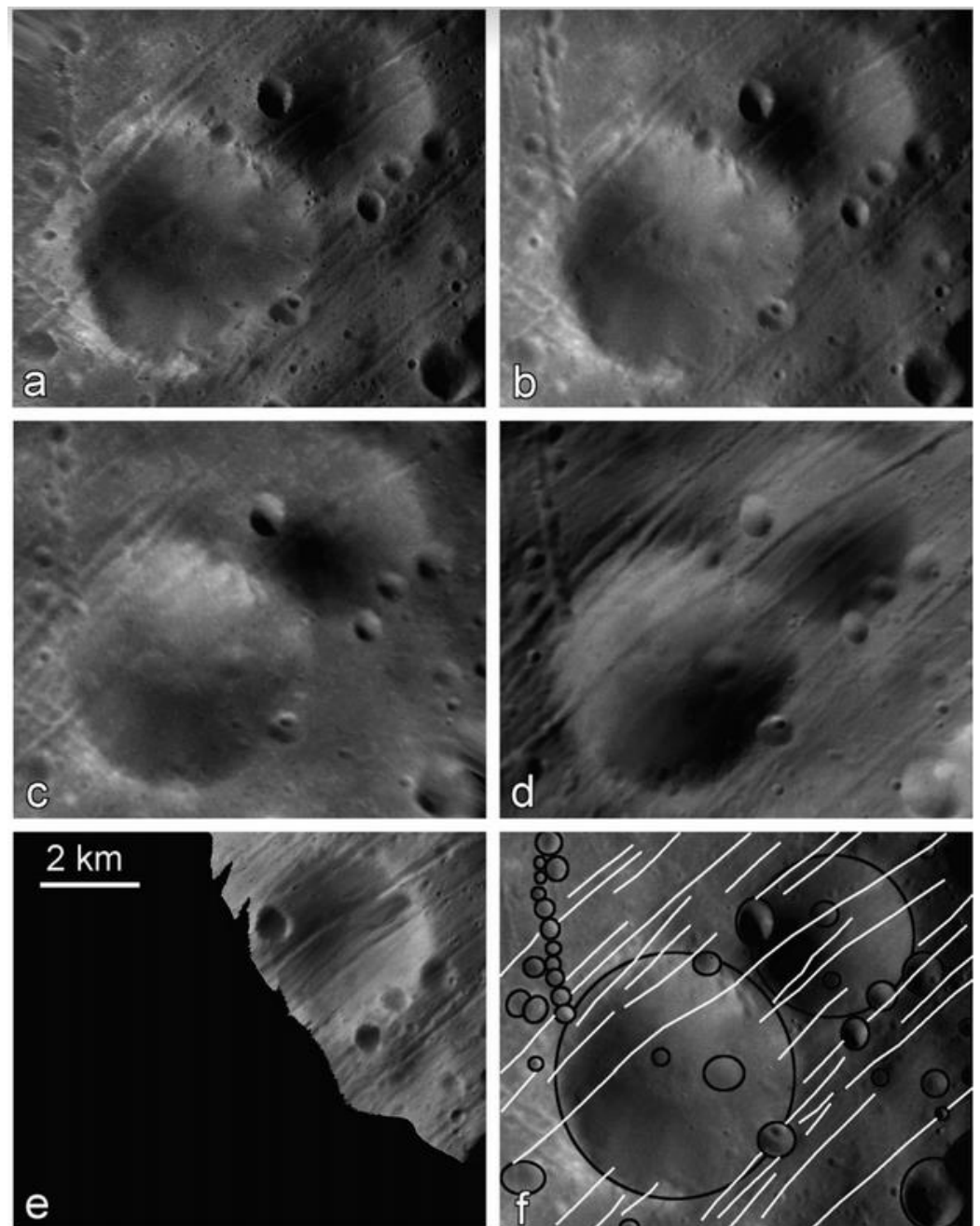
Figure 16. The HRSC images depict the craters Drunlo (bottom left) and Clustril (top right), showing fragments captured during orbits 0756 (**a**), 2780 (**b**,**f**), 2813 (**c**), 3310 (**d**), and 5851 (**e**) [12].

There are several "families" of grooves, with grooves within a family being approximately parallel to each other with an accuracy of a few degrees. Twelve such families have been identified by Murray and Heggie [49], labeled from A to L. The surfaces of grooves from different families are oriented at various angles to each other, causing the grooves to form nearly rectangular grids in some areas (Figure 17) [49].

At the intersections of grooves with different orientations, there are no clear lateral displacements (Figure 18), unlike what is often observed at intersections of different tectonic features. Some families are spatially extensive, covering areas with a meridional or longitudinal extent greater than 90–120° [12].
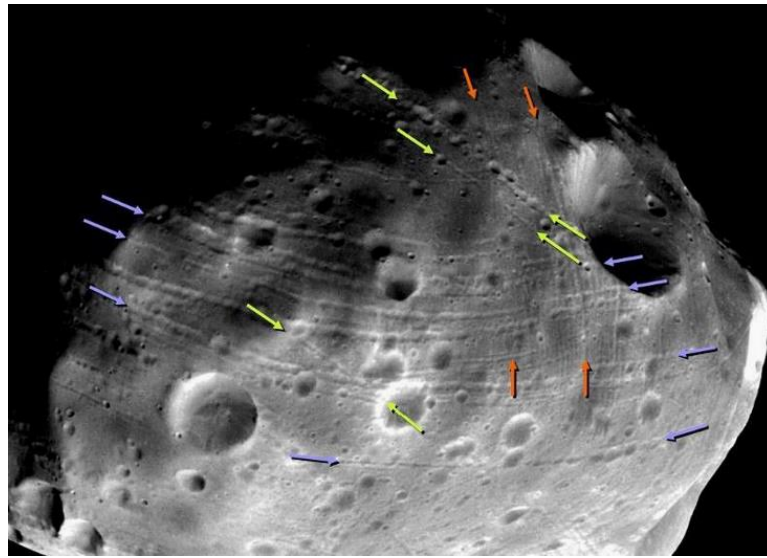
Figure 17. The image of Phobos illustrates three "families" of grooves. The orange color represents the C groove family, the yellow color represents the D groove family, and the purple color represents the F groove family. Groove families C and F intersect nearly perpendicularly near the center of the leading hemisphere, while family D (yellow arrows) intersects the other two at an angle of approximately 45°. The right half of the image, where groove families overlap, constitutes the "overlap zone". Image credit: ESA/DLR/FUB, h4847nd [49].

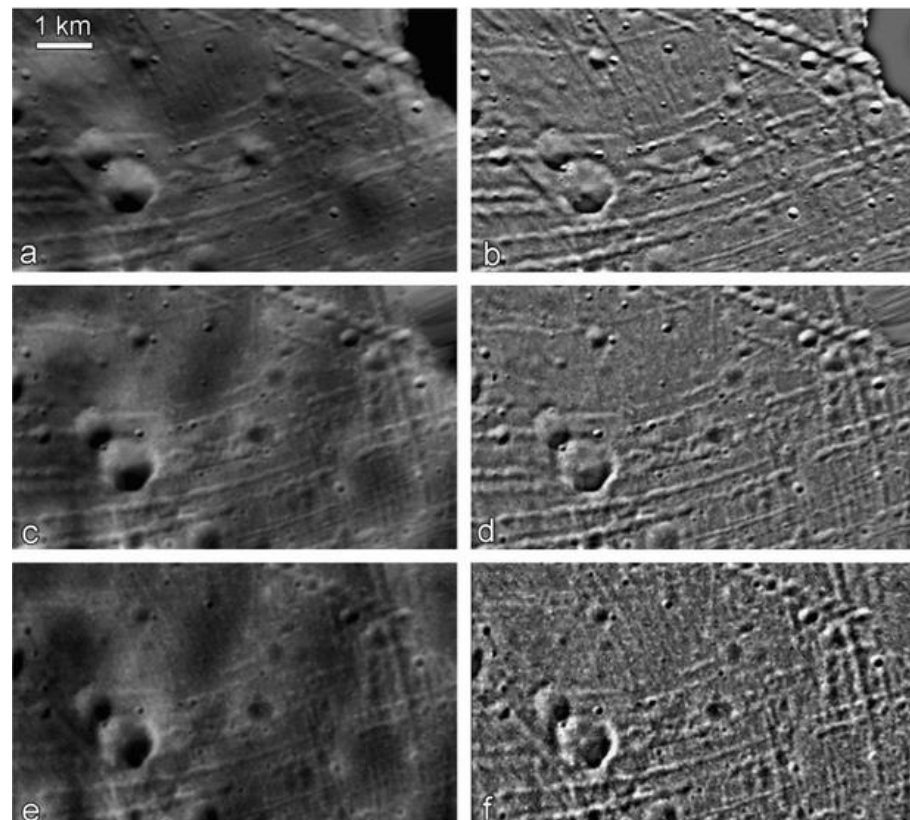**Figure 18.** Intersections of grooves southwest of the Drunlo crater. Fragments of images taken during orbits 6906 (**a**,**b**), 4847 (**c**,**d**), and 2813 (**e**,**f**); on the left—original images; on the right—stretched images to enhance contrast [12].

Grooves similar to those on Phobos are also observed on other small bodies, such as Eros, Lutetia, and Vesta. In terms of morphology and size, the grooves on Eros most closely resemble those on Phobos. Grooves on the asteroid Lutetia are morphologically similar to those on Phobos but are much wider and relatively short. Meanwhile, grooves on Vesta are even larger and more continuous [12,46].

5.3. Blocks and Boulders

Another morphological feature on the surface of Phobos includes blocks and boulders (Figure 19). Similar to the Moon, it is believed that these features originated from impact cratering on the Martian moon. They were first identified in images captured by the Viking Orbiter. The smallest blocks observed at that time had a diameter of 15–30 m, while the largest, observed inside the Stickney crater, had a diameter of 100 m [12].
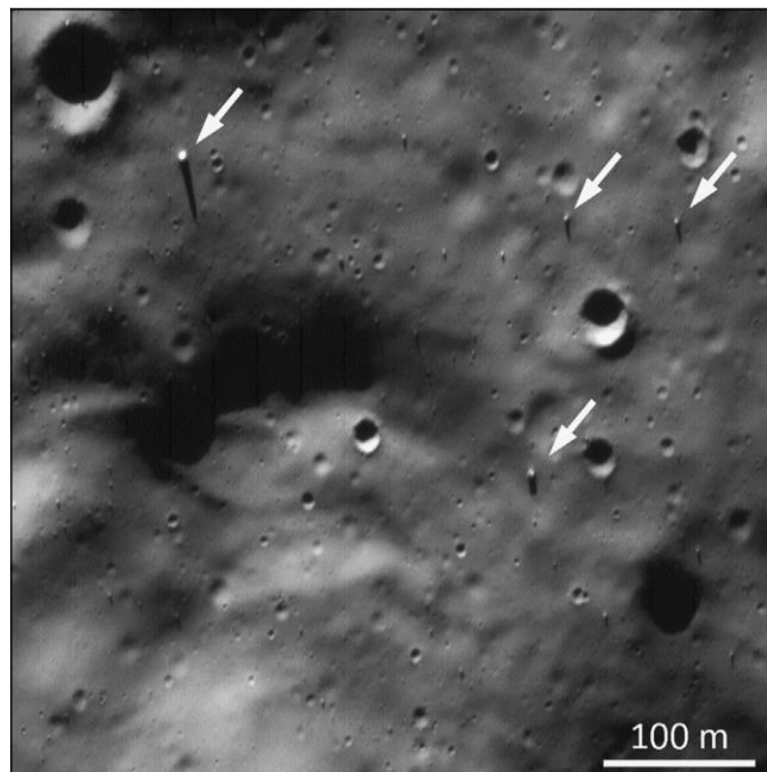

Figure 19. Boulders (white arrow) with diameters ranging from a few meters on the surface of Phobos. Image excerpt from MGS 55103 [12].

In the MGS 55103 image, covering an area of 16 km^2 (Figure 19), 900 rock fragments with diameters ranging from 2 to 16 m were counted [12].

Shingareva and Kuzmin [53] also counted less-visible, meter-sized protrusions interpreted as blocks covered with regolith or partially destroyed by micrometeoroid impacts. These meter-sized blocks are randomly distributed around small craters and on their edges, sometimes forming small chains and clusters [53].

Additionally, a shortage of boulders, responsible for creating grooves, has been observed. Wilson and Head [50] suggest the possibility of rock blocks escaping from Phobos' surface due to varying gravity and escape velocities. They state that some blocks, after forming grooves on a surface with higher gravity, may leave Phobos' surface upon reaching an area with lower escape velocity.

The missing boulders, after creating grooves, could have been removed or fragmented in subsequent years and centuries due to secondary impacts from boulders originating from the Stickney crater [51]. It is highly likely that fragments of boulders are present on Phobos but buried in regolith.

6. Characteristics and Physical Properties of Phobos Regolith

6.1. Characteristics of Phobos Regolith

The surface of Phobos, similar to the surfaces of solid bodies in the Solar System, is covered with regolith—a fragmented and unconsolidated material composed of crushed rock and soil. Regolith is formed through various impact processes, erosion, and weathering, resulting in a mixture of particles with different shapes and sizes. The outer layer of regolith is continually modified by solar wind, cosmic radiation, and meteoroid impacts. However, the processes involved in regolith formation on small bodies due to these factors have not been sufficiently studied [16].

The formation process of regolith on Phobos takes into account multiscale, multistage, and repetitive processes, including impact fragmentation, material melting, cratering with ejection, and mixing (accumulation of material both from the direct settling of ejecta and the return of high-velocity ejected fragments to the space near Mars), as well as cosmic weathering [12,13]. As a result, Phobos' surface should be covered by an unsorted mixture of solid rock fragments and material melted under the influence of impacts, with sizes ranging from micrometers to meters [12].

However, unlike the Moon, Phobos' orbital configuration allows almost all ejecta to re-impact it. Within approximately 1000 years after the collision that formed the Stickney crater, material was ejected at high speed from Stickney, then re-impacted Phobos' surface, strongly transforming it and creating a new regolith with a global thickness of 30–50 m (about 50% of the new regolith deposit produced by Stickney is the primary ejection from Stickney, and the remaining 50% is the ejecta from secondary impacts on Stickney) [51,54].

Additionally, an important characteristic of Phobos' regolith is the suggested shortage of particles with sizes <300 μm. Particles <300 μm are particularly susceptible to orbital eccentricity changes, and if they do not re-impact Phobos shortly after being ejected, they usually get lost in interplanetary space or drift away from the orbit into the Martian atmosphere [12,13].

The proximity of Mars is a significant factor influencing the properties of regolith on Phobos. Part of the ejected material from the surface of Mars most likely settles on the surface of Phobos, introducing Martian material into its regolith [16]. It is estimated that the concentration of Martian material is 250 ppm in the upper part (0.5 m) and one to two orders of magnitude lower in concentration at greater depths [12]. Analysis of the work of Ramsley and Head [13] indicates that the most probable mass concentration of Mars-ejected fragments in the contemporary Phobos regolith is around 250 ppm within the range of 20–1250 ppm.

Moreover, the thickness of Phobos' regolith, determined based on crater morphology, ejecta distribution, smooth sediment morphology, geological feature morphology such as boulders and lineaments, and spectro-photometric changes on the surface [55], is as follows:

- 5 m minimum;
- 100 m maximum [12,56].

Moreover, the size of Phobos' craters with complex morphology indicates the presence of layered material, implying the existence of a regolith layer covering the bedrock. Layers within the regolith are likely not continuous but resemble lenses. The presence of layers in the regolith is also suggested by observations of material ejected from craters, showing varying apparent brightness [12].

Additionally, the observed population of impact craters indicates that the upper several hundred meters to several kilometers of Phobos' surface are heavily fractured [12].

6.2. Physical Properties of Regolith

6.2.1. Grain Size

The surface of Phobos is most likely covered with an unsorted mixture of solid rock fragments and material melted under the influence of impacts, ranging in size from micrometers to meters, with a suggested deficiency of fractions smaller than 0.3 mm [12].

There is also an assumed difference in the maturity of Phobos' regolith between the leading and trailing hemispheres [57]. However, this difference is not apparent in higher-resolution images. This apparent homogeneity could be explained by limited image resolution or particle homogenization due to horizontal surface movements. As reported by Ballouz et al. [58], periodic dynamic changes driven by the eccentricity of the orbit, or by seasonal variations, might contribute to this phenomenon. However, it is not ruled out that this apparent homogeneity is related to a dust layer (grain size ~0.1 mm) that could have covered Phobos' surface [59,60].

Additionally, based on the surface thermal inertia (40–70 $\mathrm{Jm^{-2} \cdot K^{-1} \cdot S^{-1/2}}$—Viking observations; 20–40 $\mathrm{Jm^{-2} \cdot K^{-1} \cdot S^{-1/2}}$—Phobos 2 observations) it has been estimated that the average grain size should be smaller than 2 mm in most regions [61,62]. Sakatani et al. [63] assume a surface thermal inertia of 55 $\mathrm{Jm^{-2} \cdot K^{-1} \cdot S^{-1/2}}$, which gives them the most probable grain diameter below 1 mm.

6.2.2. Density

Measurements conducted as part of the radio-science experiment (MaRS) on Mars Express significantly improved the estimation of Phobos' mass [25,64]. This improvement was attributed to both the elliptical orbit of MEX (Mars Express—ESA's mission to the Red Planet) and refined ephemerides for Phobos, derived from the Super Resolution Camera (SRC) on board MEX [1,65]. The size of Phobos was more precisely determined thanks to images from the HRSC/SRC cameras [7,66].

Utilizing gravitational parameter (GM) estimates derived from Pätzold et al.'s work [8] (GM obtained from spacecraft tracking during flybys or long-term planetary motion integration) and the volume estimated by Willner et al. [7] (5742 ± 35 $\mathrm{km^3}$), the average volumetric densities of Phobos were determined (Table 3). Densities were calculated only for masses where the mean GM value fell within the 3σ range, with GM obtained from the close flybys of MEX 2008 ROB ($7.11 \pm 0.09 \times 10^{-4}$ $\mathrm{km^3 \cdot s^{-2}}$). The resulting density values fall within the range of 1845—1880 $\mathrm{kg/m^3}$ (1857 $\mathrm{kg/m^3}$—mean value) (Table 3, Figure 20).

Table 3. GM values and the corresponding calculated masses and volumetric densities.

Database	GM $\times 10^{-4}$ $\mathrm{km^3\ s^{-2}}$	Error $\times 10^{-4}$ $\mathrm{km^3\ s^{-2}}$	Source of Adopted GM	Mass [1] $\times 10^{16}$ kg	Error $\times 10^{16}$ kg	Volume Density [2] $\mathrm{kg/m^3}$	Error $\mathrm{kg/m^3}$
			Close spacecraft flybys				
Phobos-2	7.163	±0.0080	[8,67]	1.0732	±0.0012	1869	±12
Viking	7.1260	±0.0450	[15]	1.0677	±0.0067	1859	±16
Viking (w/o nongrav)	7.0770	±0.0030	[15]	1.0603	±0.0004	1847	±11
Phobos-2	7.0910	±0.0050	[15]	1.0624	±0.0007	1850	±11
Phobos-2 (w/o nongrav)	7.0910	±0.0050	[15]	1.0624	±0.0007	1850	±11
Viking and Phobos-2	7.0920	±0.0040	[15]	1.0626	±0.0006	1851	±11
Mars Express (MEX) 2006	7.1200	±0.1200	[25]	1.0668	±0.0180	1858	±33
Mars Express (MEX) 2008 (UniBw)	7.1270	±0.0210	[25]	1.0678	±0.0031	1860	±13
Mars Express (MEX) 2008 (ROB)	7.1100	±0.0300	[25]	1.0653	±0.0045	1855	±14
Mars Express (MEX) 2010 (with C20)	7.0720	±0.0140	[68]	1.0596	±0.0021	1845	±12
Mars Express (MEX) 2010 (GM only)	7.0840	±0.0070	[68]	1.0614	±0.0010	1848	±11
Mars Express (MEX) 2010 and 2013	7.0765	±0.0075	[69]	1.0603	±0.0011	1847	±11
			Gravity field solutions				
Mars50b, Viking	7.1060	±0.0130	[70]	1.0647	±0.0019	1854	±12
Mars50c, Viking and Mariner-9	7.0900	±0.0120	[70]	1.0623	±0.0018	1850	±12
MGS75D, Mars Global Surveyor (MGS)	7.1380	±0.0190	[71]	1.0695	±0.0028	1863	±12
MGS95J, Mars Global Surveyor (MGS)	7.1260	±0.1140	[72]	1.0677	±0.0171	1859	±32

Table 3. *Cont.*

Database	GM $\times 10^{-4}$ km^3 s^{-2}	Error $\times 10^{-4}$ km^3 s^{-2}	Source of Adopted GM	Mass [1] $\times 10^{16}$ kg	Error $\times 10^{16}$ kg	Volume Density [2] kg/m^3	Error kg/m^3
MGS95J, Odyssey	7.2050	±0.1470	[72]	1.0795	±0.0220	1880	±40
MGS95J, MGS and Odyssey	7.1580	±0.0890	[72]	1.0725	±0.0133	1868	±26
MRO110B and MRO110B2, many missions (MGS, Odyssey, MRO, Pathfinder, Viking landers)	7.1700	±0.0700	[73]	1.0743	±0.0108	1871	±22
Distant encounters							
Mars Express (MEX)	7.1100	±0.0200	[57]	1.0653	±0.0030	1855	±12
Phobos average volumetric density						1857	±17

[1] Gravitational constant G = 6.67430(15) $\times 10^{-11}$ m$^3 \cdot$kg$^{-1} \cdot$s^{-2} [74]. [2] Volume 5742 ± 35 km^3 [7].
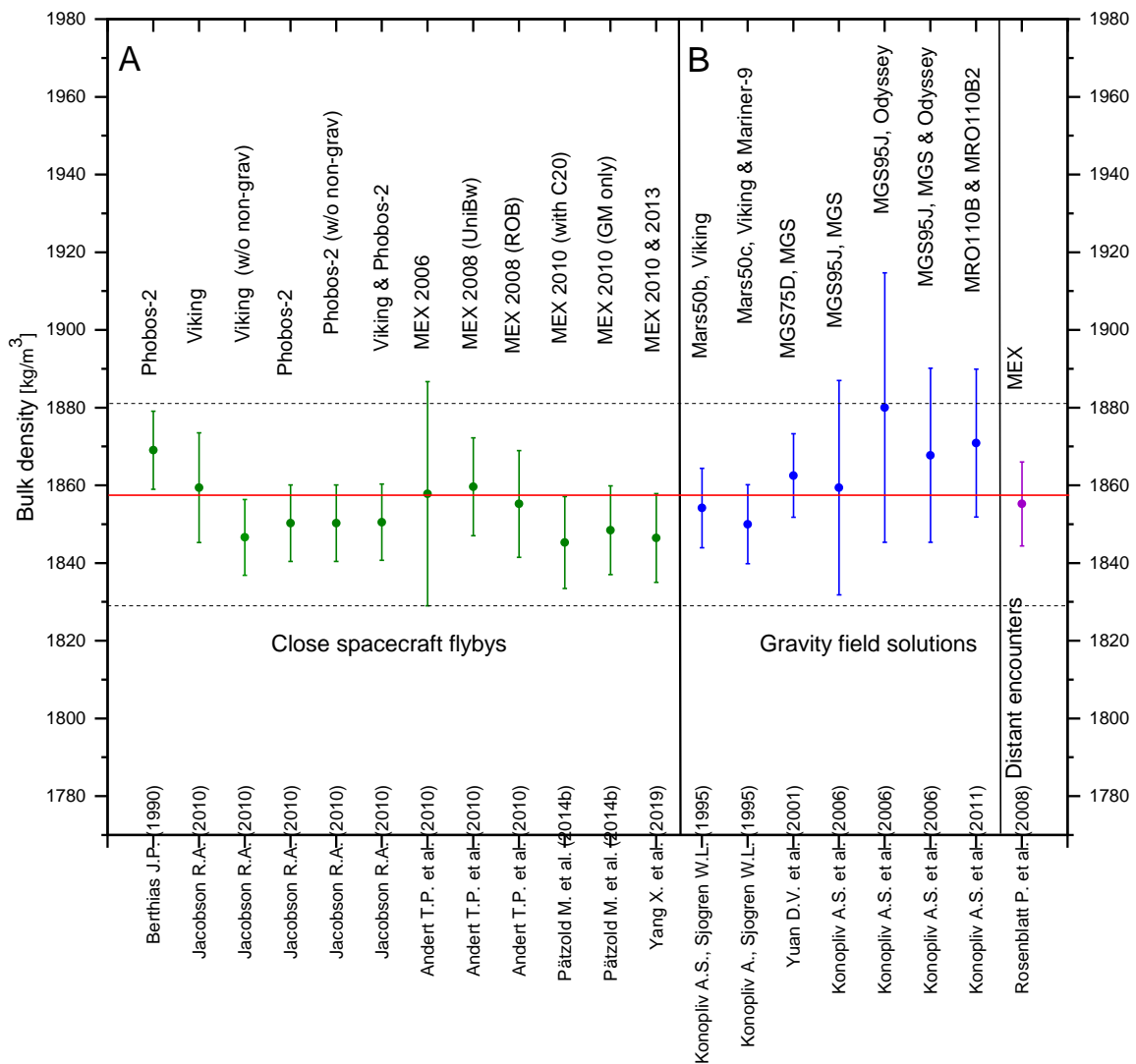

Figure 20. The volumetric density of Phobos was determined using a volume of 5742 ± 35 km^3 [7] and mass obtained from (**A**) GM derived from close spacecraft flybys, (**B**) GM derived from the gravitational field of Mars or distant perturbations in the spacecraft's orbit. The volumetric density was calculated only using masses for which the average value of GM fell within the range of 3σ of the GM obtained from the close flybys of MEX 2008 ROB [8]. The horizontal dashed lines represent the upper and lower bounds of the 3σ error associated with the volumetric density derived from the GM of MEX 2008 ROB [8].

The volumetric density of Phobos was calculated based on the mass values from MEX 2008 UniBw (German Armed Forces in Munich) [25,68] and the mass from the MEX 2010 flyby (with C20—second-degree gravity coefficients) [68], resulting in densities of 1860 kg/m^3 ($\pm$13 kg/m^3) and 1845 kg/m^3 ($\pm$12 kg/m^3) (Table 3, Figure 20). When using the same volume but considering the masses from the MEX 2010 and 2013 flybys [69], the volumetric density was found to be 1847 kg/m^3 ($\pm$11 kg/m^3) (Table 3, Figure 20).

For the GM determined within the uncertainty range, which accounts for most solutions from flybys, gravity field derivations, and "distant" encounters [8], or the ROB (Royal Observatory of Belgium) solution from the close MEX 2008 flyby but with a range of $\pm 3 \times 0.03 \times 10^{-4}$ km^3·s^{-2}, the volumetric density was calculated to be 1855 kg/m^3 ($\pm$26 kg/m^3).

Comparing the volume density of Phobos to the density of other asteroids and meteorites (Figure 21), it can be observed that it is similar to the density of low-albedo carbonaceous asteroids (falling roughly in the middle of their density range, Figure 21). Available volume density data for asteroids indicate that they are generally lower than the density of their carbonaceous meteorite analogs, much like the volume density of Phobos, which is also lower than most carbonaceous material samples (Figure 20).

Additionally, based on surface observations of Phobos conducted by the Arecibo radar system, Busch et al. [75] estimated the volume density of the uppermost layer to be approximately 1600 $\pm$ 300 kg/m^3. This density is similar to the density of Cl chondritic meteorites Cl (1.6 $\pm$ 0.03 g/cm^3) [70] and the Tagish Lake meteorite (1.64 $\pm$ 0.02 g/cm^3) [76] (Figure 21), which is most likely a fragment of a D-type asteroid.
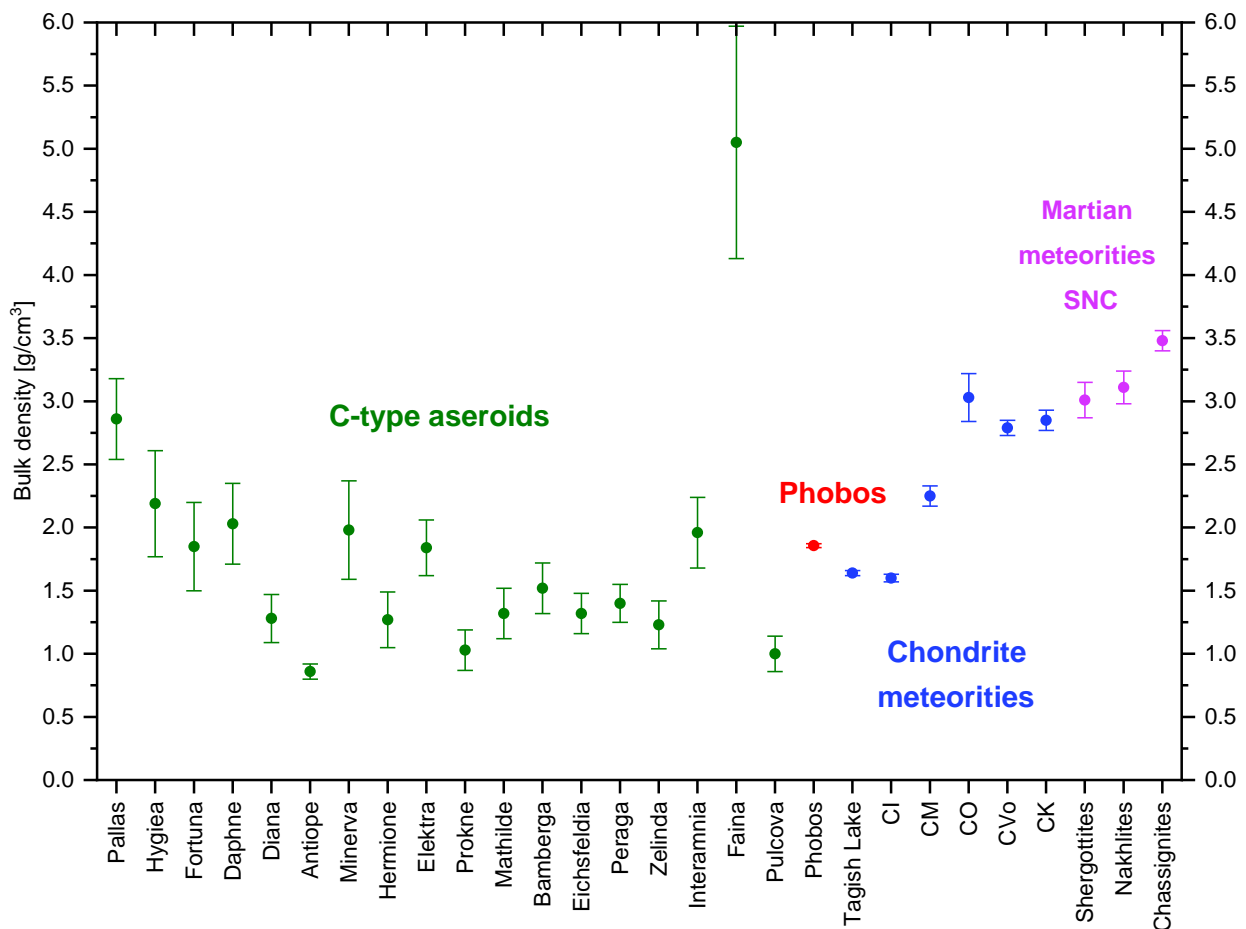

Figure 21. The volume density of Phobos (average density, Table 3) compared with low-albedo carbonaceous asteroids (C-type asteroids) [77], chondritic meteorites [76], and Martian meteorites (SNC) [73].

6.2.3. Porosity

The low bulk density of Phobos (average value of 1857 kg/m^3, Table 3) can be explained by its relatively high porosity and/or the presence of light materials, such as water ice, within its interior [1,68].

Rosenblatt [1], to determine the porosity of Phobos, assumed that its rocky interior corresponds to a single material with a bulk density ρ_a (Table 4) and that there is no light material inside the pores. With this assumption, the porosity (n) needed to achieve the determined bulk density ρ_b (1857 kg/m^3, Table 3) can be expressed by the formula

$$n = 1 - \frac{\rho_b}{\rho_a},\qquad(1)$$

The calculated porosity does not account for the inherent porosity of the rocks constituting the moon but only corresponds to the void spaces between potentially constituting rock blocks (macroporosity).

Using a broad range of density values for analogs that could potentially compose Phobos (Table 4), a macroporosity ranging from 17.47% to 46.64% was determined (Figure 3). Assuming an analog of hydrated carbonaceous material, a porosity of approximately 17.5% is obtained. This is less than the range of 40% to 60% reported for C- type asteroids constructed from hydrated carbonaceous material [76]. For analogs of silicate materials, the estimated porosity value is higher than that for hydrated carbonaceous material, reaching around 47% (SNC achondrites, upper limit, Table 4, Figure 22), similar to the obtained porosity value for black chondrite (around 45%). These values are significantly higher than the porosity range estimated for S-type asteroids (20–30% or less, except for near-Earth asteroids, which have a macroporosity estimated at around 40% [76]). Moreover, the density of Tagish Lake is lower than the volumetric density of Phobos, suggesting that achieving the average volumetric density determined for Phobos (1857 kg/m^3, Table 3) would require compressing the Tagish Lake material.
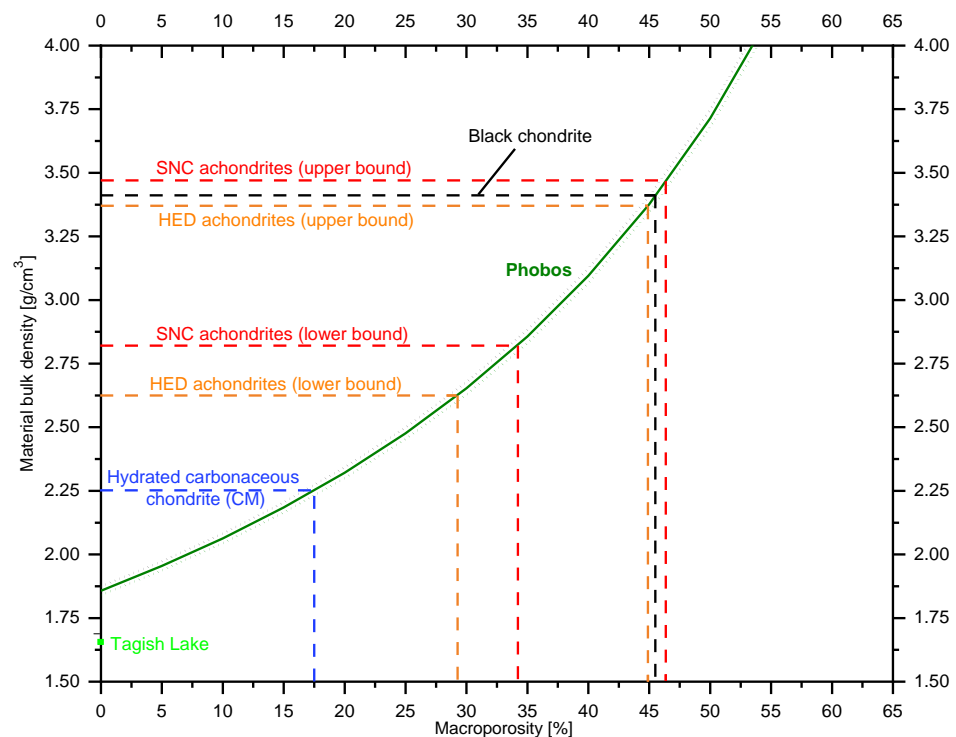

Figure 22. The macroporosity of Phobos (dark green curve) estimated based on the bulk densities of analog rock materials, which it may hypothetically be composed of (Table 4), with an error range (dark-green dashed curve) (partially based on [1]).

Table 4. Densities of materials that could form Phobos and their corresponding porosities.

Types of Analog Materials [1]	Bulk Density [g/cm^3]	Range +/− [g/cm^3]	Source	Phobos Macroporosity [%]	Range +/− [%]	Grain Density [g/cm^3]	Range +/− [g/cm^3]	Source	Total Porosity of Phobos [%]	Range +/− [%]
Hydrated Carbonaceous Chondrite (CM)	2.25	0.08	[76]	17.47	3.03	2.9	0.08	[76]	35.97	1.86
Tagish Lake	1.64	0.02	[78]	—	—	2.72	—	[78]	31.73	—
Black Chondrite	3.39	0.045	[79]	45.22	0.88	3.5	0.025	[79]	46.94	0.62
HED Achondrites (Asteroidal) (Lower Limit)	2.62	—	[80]	29.12	—	2.99	—	[80]	37.89	—
HED Achondrites (Asteroidal) (Upper Limit)	3.37	—	[80]	44.90	—	3.51	—	[80]	47.09	—
SNC Achondrites (Martian Meteorites) (Lower Limit)	2.83	—	[80]	34.38	—	3.08	—	[80]	39.71	—
SNC Achondrites (Martian Meteorites) (Upper Limit)	3.48	—	[80]	46.64	—	3.73	—	[80]	50.21	—

[1] Types of analog materials adopted from Rosenblatt [1], except for SNC achondrites.

Basing the analysis on grain density instead of volumetric density, a total porosity ranging from 31.73% to 50.21% was obtained (Table 2, Figure 23). These values align well with the porosity of C-type asteroids (40–60%).
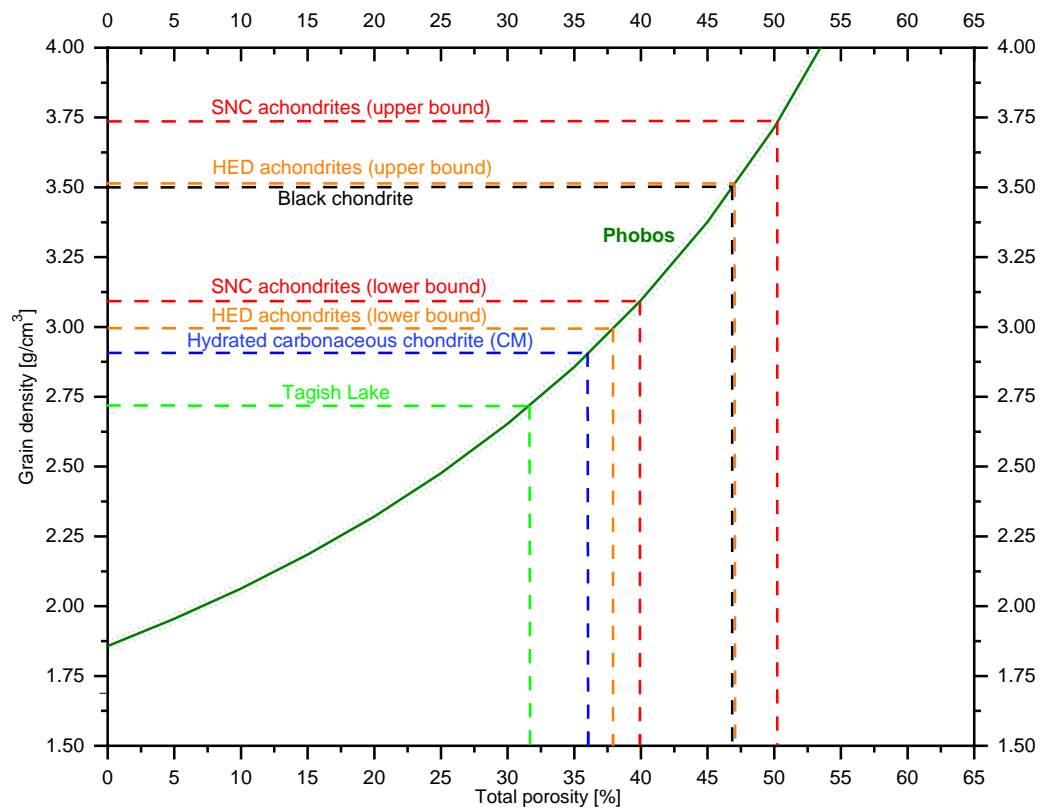

Figure 23. The total porosity of Phobos (dark green curve) estimated based on the grain density of analog materials, which might hypothetically constitute the moon (Table 4), with an error range (dark-green dashed curve).

The presence of significant porosity/macro porosity is confirmed by the existence of the Stickney crater on Phobos' surface [1,25]. The formation of such large craters on a small body (roughly the diameter of the body) requires substantial porosity to prevent the body from being destroyed during the impact process [81]. The high macro porosity of Phobos indicates that its interior does not correspond to a monolithic rock but rather to a gravitationally loosely consolidated assemblage of materials [81].

6.2.4. Water Ice

Although no evidence of water has been observed on the surface of Phobos, it cannot be ruled out that its interior contains a certain amount of water ice. The temperature conditions inside Phobos do not exclude its presence, and the regolith covering the surface may protect it from sublimation and transport to the surface in large quantities [1].

Depending on the density of the analog rocky material, water ice will occupy a different volume. The density of the analog rocky material ρ_{rock}, depending on the amount of water ice and porosity, can be calculated using the relationship [8]

$$\rho_{rock} = \frac{\rho_b - \rho_{ice} \cdot wi}{1 - n - wi} \tag{2}$$

where ρ_b is the average volumetric density of Phobos (1857 kg/m^3, Table 3), ρ_{ice} is the density of water ice (0.97 g/cm^3), wi is the water ice content, and n is the volumetric porosity.

On Figure 24, the density of the analog rocky material is presented as a function of porosity and water ice content, calculated from Equation (2). Depending on the density of

the analog rocky material and considering the porosity given in Andert et al. [25], ranging from 25–35% (30 ± 5%), water ice may constitute from about 0% to about 20% of Phobos' mass (Figure 24). Assuming a porosity of 25–35% and a 0% water ice content, the required density of the rocky material should fall within the range of 2.48–2.86 g/cm^3. These values are consistent with the densities of materials such as hydrated carbonaceous chondrites. On the other hand, for a 20% water ice content, the density of the rocky material should range from 3.02 g/cm^3 to 3.70 g/cm^3, corresponding to the densities of silicate material or black chondrites. Assuming a porosity of 25%–30%, the water ice content could even reach 30%.
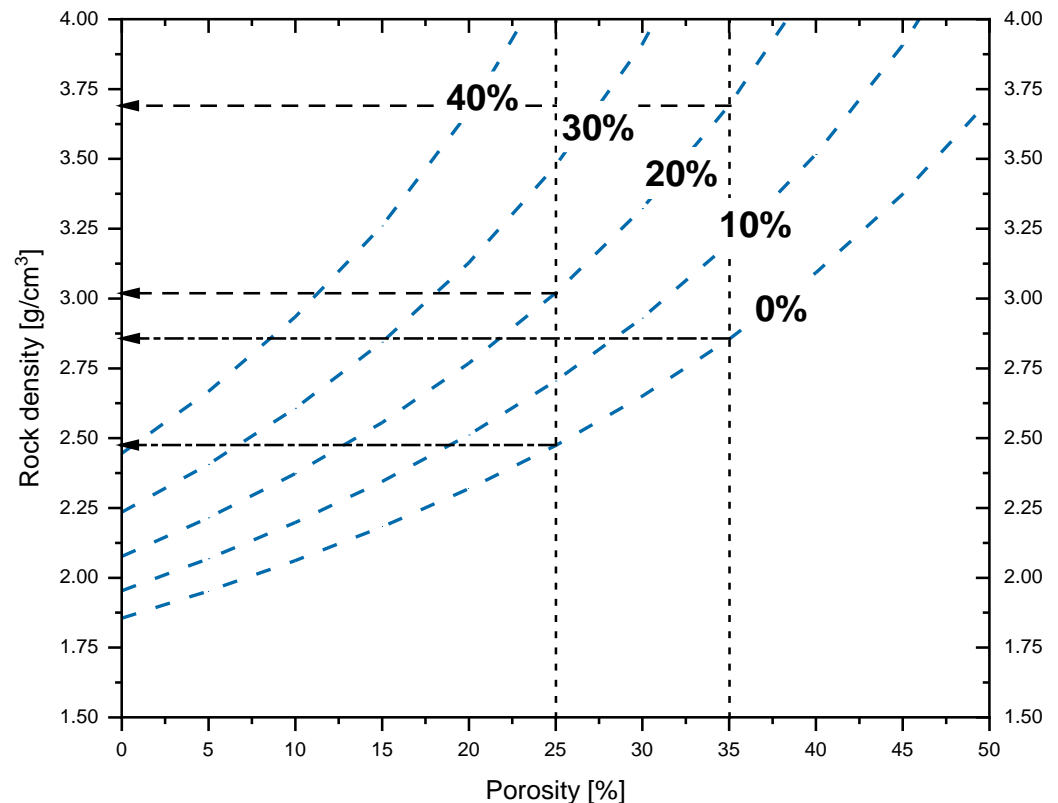

Figure 24. The density of the rocky material as a function of porosity and water ice content according to equation (2) (modified graph from Pätzold et al. [8]).

7. Conclusions

In the process of evolution, all planets and most of their satellites undergo various changes due to external factors and endogenic processes. These processes have radically transformed the building blocks of planets and almost entirely altered the original material. However, smaller bodies in the Solar System, such as Phobos, due to their small size and normal levels of radioactive isotopes, exclude internal heat and endogenous tectonic activity. Therefore, these bodies serve as a source of raw materials similar to the primordial cloud substance from which the planets of the Solar System originated [16].

Additionally, each planetary system exhibits unique features. For instance, the Martian system lacks a single large moon, like Earth, or multiple moons of varying sizes, as found around giant planets. Instead, it possesses two small moons: Phobos and Deimos. The formation mechanism of such a system is still under investigation [14].

There are two main hypotheses explaining the origin of Phobos, the first being the capture hypothesis, e.g., [18,20], and the second, the in situ formation hypothesis, e.g., [17,23]. Currently, the capture hypothesis is considered less likely. This is associated, among other factors, with the fact that dynamic capture models require specific conditions, including aerodynamic resistance in the early proto-atmosphere of Mars [4,10,18,20]. On the other

hand, numerical simulations conducted to replicate the complete scenario of the in situ formation hypothesis (impact, accretion, and long-term evolution of two moons) show better agreement with the current orbits than the capture hypothesis, and they are consistent with observations regarding their presumed composition [14].

Despite the lack of precise data on Phobos's composition, scientists, based on hypotheses about its formation, have proposed a hypothetical composition. If Phobos is a captured asteroid, then most of its mass may consist of primitive carbonaceous material (possibly a cousin of D-type bodies from the outer asteroid belt). However, if Phobos formed due to a giant impact (high-energy collision), it should be composed of roughly half Martian material and half impactor material [34].

The available spectroscopic data indicate the presence of two distinct materials on the surface of Phobos, namely areas with different spectral slopes—red and blue units. The red unit covers the majority of the moon's surface, while the blue unit is exposed near the Stickney crater [10]. Spectral observations highlight the ambiguity of Phobos's composition, where reflectance spectra suggest the presence of carbonaceous material [37], while emissivity spectra indicate the presence of silicates [40]. The composition of Phobos remains uncertain.

The current preferred model for Phobos, in line with available observational data, suggests that it is primarily a heterogeneous object consisting of a mixture of red and blue material blocks of varying sizes [12].

The surface of Phobos is characterized by numerous craters (1300 craters with a diameter greater than 200 m [12]), grooves (12 families of grooves [49]), as well as blocks and rocky boulders. Its surface is most likely covered with an unsorted mixture of solid rock fragments and impact-melted material, ranging in size from micrometers to meters, with a suggested deficiency in fractions smaller than <0.3 mm (e.g., [12]). However, it is not excluded that a thin layer of dust (grain size ~0.1 mm) may cover its surface layers [59,60].

Additionally, it is estimated that the average grain size of the regolith should be smaller than 2 mm in most regions of Phobos (thermal inertia of the surface 40–70 $Jm^{-2} \cdot K^{-1} \cdot S^{-1/2}$ and 20–40 $Jm^{-2} \cdot K^{-1} \cdot S^{-1/2}$) [61,62]. Assuming a surface thermal inertia of 55 $Jm^{-2} \cdot K^{-1} \cdot S^{-1/2}$, the most probable grain diameter should be below 1 mm [63].

The density values of Phobos, obtained based on the gravitational mass estimates (GM) from Pätzold et al. [8] and the volume provided by Willner et al. [7], fall within the range of 1845–1880 kg/m^3 (1857 kg/m^3—average value) (Table 3, Figure 20). Comparing the bulk density of Phobos to the densities of other asteroids and meteorites, it can be observed that it is similar to the density of C-type asteroids. However, Busch et al. [75] estimated the bulk density of the top several tens of centimeters of the surface layer to be around 1600 ± 300 kg/m^3. This density is similar to the densities of CI chondrite meteorites and the Tagish Lake meteorite, which is most likely a fragment of a D-type asteroid.

Phobos is suspected to be highly porous, indicated by the presence of the Stickney crater on its surface [1,25]. The formation of such large craters on a small body requires significant porosity, preventing the body from being destroyed during the impact process [81]. Utilizing grain densities (Table 4), the total porosity of Phobos was determined to be in the range of 31.73–50.21% (Table 4, Figure 23). These values closely mirror the porosity of C-type asteroids (40–60%).

Although scientific research conducted through a spacecraft orbiting Mars (currently or in the past) has provided valuable information about Phobos, there are still gaps in our knowledge about it. Despite attempts to estimate Phobos' composition (spectroscopic data, high-resolution imaging), its composition remains unknown. It is known that two main materials (red and blue units) occur throughout its surface, but their properties, distribution, and spatial relationships are unknown. Additionally, the physical parameters of the regolith are only approximate, and its origin remains an open question.

Acquiring detailed knowledge about Phobos would allow, among other things, resolving questions about its origin, understanding the geochemical processes occurring on it, comprehending the early geological history of Mars' environment, and preparing for future

crewed missions. However, determining the composition of Phobos, and, consequently, its origin, requires additional information about its mineralogical, elemental, and isotopic composition, which would need to be obtained through in situ studies or collected samples.

References

1. Rosenblatt, P. The origin of the Martian moons revisited. *Astron. Astrophys. Rev.* **2011**, *19*, 44. [CrossRef]
2. Oberst, J.; Zakharov, A.; Schulz, R. Why Study Phobos and Deimos? An Introduction to the Special Issue. *Planet. Space Sci.* **2014**, *102*, 1. [CrossRef]
3. Duxbury, T.C.; Zakharov, A.V.; Hoffmann, H.; Guinnes, E.A. Spacecraft exploration of Phobos and Deimos. *Planet. Space Sci.* **2014**, *102*, 9–17. [CrossRef]
4. Murchie, S.L.; Britt, D.T.; Pieters, C.M. The value of Phobos sample return. *Planet. Space Sci.* **2014**, *102*, 176–182. [CrossRef]
5. Archinal, B.A.; A'Hearn, M.F.; Bowell, E.; Conrad, A.; Consolmagno, G.J.; Courtin, R.; Fukushima, T.; Hestroffer, D.; Hilton, J.L.; Krasinsky, G.A.; et al. Report of the IAU Working Group on cartographic coordinates and rotational elements: 2009. *Celest. Mech. Dyn. Astron.* **2011**, *109*, 101–135. [CrossRef]
6. Archinal, B.A.; Acton, C.H.; A'Hearn, M.F.; Conrad, A.; Consolmagno, G.J.; Duxbury, T.; Hestroffer, D.; Hilton, J.L.; Kirk, R.L.; Klioner, S.A.; et al. Report of the IAU Working Group on Cartographic Coordinates and Rotational Elements: 2015. *Celest. Mech. Dyn. Astron.* **2019**, *130*, 22. [CrossRef]
7. Willner, K.; Shi, X.; Oberst, J. Phobos' shape and topography models. *Planet. Space Sci.* **2014**, *102*, 51–59. [CrossRef]
8. Pätzold, M.; Andert, T.; Jacobson, R.; Rosenblatt, P.; Dehant, D. Phobos: Observed bulk properties. *Planet. Space Sci.* **2014**, *102*, 86–94. [CrossRef]
9. Jet Propulsion Laboratory, NASA. Available online: https://www.jpl.nasa.gov/images/pia10368-phobos-from-6800-kilometers-color (accessed on 7 March 2024).
10. Fraeman, A.A. Materials and Surface Processes at Gale Crater and the Moons of Mars Derived from High Spatial and Spectral Resolution Orbital Datasets. Ph.D. Thesis, Washington University, St. Louis, MI, USA, 2014.
11. National Academies of Sciences, Engineering, and Medicine and the European Science Foundation (NASEM). *Planetary Protection Classification of Sample Return Missions from the Martian Moons*; The National Academies Press: Washington, DC, USA, 2019. [CrossRef]
12. Basilevsky, A.T.; Lorenz, C.A.; Shingareva, T.V.; Head, J.W.; Ramsley, K.R.; Zubarev, A.E. The surface geology and geomorphology of Phobos. *Planet. Space Sci.* **2014**, *102*, 95–118. [CrossRef]
13. Ramsley, K.R.; Head, J.W. Mars impact ejecta in the regolith of Phobos: Bulk concentration and distribution. *Planet. Space Sci.* **2013**, *87*, 115–129. [CrossRef]
14. Rosenblatt, P.; Hyodo, R.; Pignatale, F.; Trinh, A.; Charnoz, S.; Dunseath, K.M.; Dunseath-Terao, M.; Genda, H.; The Formation of the Martian Moons. Final Manuscr. *Oxf. Sci. Encycl.* 2019. Available online: https://www.researchgate.net/publication/335713198 (accessed on 15 March 2024).
15. Jacobson, R.A. The orbits and masses of the Martian satellites and the liberation of Phobos. *Astron. J.* **2010**, *139*, 668–679. [CrossRef]
16. Zelenyi, L.M.; Zakharova, A.V.; Polischuk, G.M.; Martynov, M.B. Project of the Mission to Phobos. *Sol. Syst. Res.* **2010**, *44*, 15–25. [CrossRef]
17. Burns, J.A. Contradictory Clues as to the Origin of the Martian Moons. In *Mars*; Kieffer, H., Jakosky, B., Snyder, C., Matthews, M., Eds.; University of Arizona Press: Tucson, AZ, USA, 1992; pp. 1283–1301.
18. Sasaki, S. Origin of Phobos: Aerodynamic drag capture by the primary atmosphere of Mars. *Abstr. Lunar Planet. Sci. Conf.* **1990**, *21*, 1069–1070.
19. Kilgore, T.R.; Burns, J.A.; Pollack, J.B. Orbital evolution of "Phobos" following its "capture". *Am. Astron. Soc.* **1978**, *10*, 593.
20. Hunten, D.M. Capture of Phobos and Deimos by photo atmospheric drag. *Icarus* **1979**, *37*, 113–123. [CrossRef]
21. Kaula, W.M. Tidal Dissipation by Solid Friction and the Resulting Orbital Evolution. *Rev. Geophys. Space Phys.* **1964**, *2*, 661–685. [CrossRef]
22. Szeto, A.M.K. Orbital evolution and origin of the Martian satellites. *Icarus* **1983**, *55*, 133–168. [CrossRef]

23. Peale, S.J. The origin of the natural satellites. *Treatise Geophys.* **2007**, *10*, 465–508. [CrossRef]
24. Craddock, R.A. The Origin of Phobos and Deimos by a giant impact. In Proceedings of the EPSC-DPS Joint Meeting, Nantes, France, 2–7 October 2011.
25. Andert, T.P.; Rosenblatt, P.; Paetzold, M.; Haeusler, B.; Dehant, V.; Tyler, G.L.; Marty, J.C. Precise mass determination and the nature of Phobos. *Geophys. Res. Lett.* **2010**, *37*, L09202. [CrossRef]
26. Bruck, S.M.; Rovny, J.; Owen, J.M.; Miller, P.L. Excavating Stickney crater at Phobos. *Geophys. Res. Lett.* **2016**, *43*, 10595–10601. [CrossRef]
27. Hurford, T.A.; Asphaug, E.; Spitale, J.N.; Hemingway, D.; Rhoden, A.R.; Henning, W.G.; Bills, B.G.; Kattenhorn, S.A.; Walker, M. Tidal disruption of Phobos as the cause of surface features. *J. Geophys. Res. Planets* **2016**, *121*, 1054–1065. [CrossRef]
28. Singer, S.F. Origin of the Martian satellites Phobos and Deimos. In Proceedings of the First International Workshop on the Exploration of Phobos and Deimos, Moffett Field, CA, USA, 5–8 November 2007; p. 7020.
29. Rosenblatt, P.; Charnoz, S. On the formation of the Martian moons from a circum-martian accretion disk. *Icarus* **2012**, *221*, 806–815. [CrossRef]
30. Craddock, R.A. Are Phobos and Deimos the result of a giant impact? *Icarus* **2011**, *211*, 1150–1161. [CrossRef]
31. Citron, R.I.; Genda, H.; Ida, S. Formation of Phobos and Deimos via a giant impact. *Icarus* **2015**, *252*, 334–338. [CrossRef]
32. Hyodo, R.; Genda, H.; Charnoz, S.; Pignatale, F.C.F.; Rosenblatt, P. On the Impact Origin of Phobos and Deimos. IV. Volatile Depletion. *Astrophys. J.* **2018**, *860*, 150. [CrossRef]
33. Pignatale, F.C.; Charnoz, S.; Rosenblatt, P.; Hyodo, R.; Nakamura, T.; Genda, H. On the Impact Origin of Phobos and Deimos. III. Resulting Composition from Different Impactors. *Astrophys. J.* **2018**, *853*, 118. [CrossRef]
34. Hyodo, R.; Genda, H.; Charnoz, S.; Rosenblatt, P. On the Impact Origin of Phobos and Deimos. I. Thermodynamic and Physical Aspects. *Astrophys. J.* **2017**, *845*, 125. [CrossRef]
35. Pieters, C.M.; Murchie, S.; Thomas, N.; Britt, D. Composition of surface materials on the moons of Mars. *Planet. Space Sci.* **2014**, *102*, 144–151. [CrossRef]
36. Fraeman, A.A.; Arvidson, R.E.; Murchie, S.L.; Rivkin, A.; Bibring, J.P.; Choo, T.H.; Gondet, B.; Humm, D.; Kuzmin, R.O.; Manaud, N.; et al. Analysis of disk-resolved OMEGA and CRISM spectral observations of Phobos and Deimos. *J. Geophys. Res.* **2012**, *117*, E11. [CrossRef]
37. Fraeman, A.A.; Murchie, S.L.; Arvidson, R.E.; Clark, R.N.; Morris, R.V.; Rivkin, A.S.; Vilas, F. Spectral absorptions on Phobos and Deimos in the visible/near infrared wavelengths and their compositional constraints. *Icarus* **2014**, *229*, 196–205. [CrossRef]
38. Lantz, C.; Clark, B.E.; Barucci, M.A.; Lauretta, D.S. Evidence for the effects of space weathering spectral signatures on low albedo asteroids. *Astron. Astrophys.* **2013**, *554*, A138. [CrossRef]
39. Vernazza, P.; Cipriani, F.; Dukes, C.; Fulvio, D.; Howard, K.T.; Witasse, O.; Brunetto, R.; Strazzulla, G.; Binzel, R.P.; Bland, P.A.; et al. Origin of the Martian moons: Investigating their surface composition. *Eur. Planet. Sci. Congr.* **2010**, *5*, 262.
40. Giuranna, M.; Roush, T.L.; Duxbury, T.; Hogan, R.C.; Carli, C.; Geminale, A.; Formisano, V. Compositional interpretation of PFS/MEX and TES/MGS thermal infrared spectra of Phobos. *Planet. Space Sci.* **2011**, *59*, 1308–1325. [CrossRef]
41. Yamamoto, S.; Watanabe, S.; Matsunaga, T. Space-Weathered Anorthosite as Spectral D-Type Material on the Martian Satellites. *Geophys. Res. Lett.* **2018**, *45*, 1305–1312. [CrossRef]
42. Marinova, M.M.; Aharonson, O.; Asphaug, E. Mega-impact formation of the Mars hemispheric dichotomy. *Nature* **2008**, *453*, 1216–1219. [CrossRef] [PubMed]
43. Canup, R.; Salmon, J. Origin of Phobos and Deimos by the impact of a Vesta-to Ceres sized body with Mars. *Sci. Adv.* **2018**, *4*, eaar688. [CrossRef] [PubMed]
44. USGS Science for a Changing World. Gazetteer of Planetary Nomenclature. Available online: https://planetarynames.wr.usgs.gov/Page/PHOBOS/target (accessed on 7 March 2024).
45. Thomas, N.; Stelter, R.; Ivanov, A.; Bridges, N.T.; Herkenhoff, K.E.; McEwen, A.S. Spectral heterogeneity on Phobos and Deimos: HiRISE observations and comparisons to Mars Pathfinder results. *Planet. Space Sci.* **2011**, *59*, 1281–1292. [CrossRef]
46. Basilevsky, A.T.; Shingareva, T.V. The Selection and Characterization of the Phobos-Soil Landing Sites. *Sol. Syst. Res.* **2010**, *44*, 38–43. [CrossRef]
47. Shingareva, T.V.; Basilevsky, A.T.; Shashkina, V.P.; Neukum, G.; Werner, S.; Jaumann, R.; Giese, B.; Gwinner, K. Morphological characteristics of the Phobos craters and grooves. In Proceedings of the 39th Lunar and Planetary Science Conference, League City, TX, USA, 10–24 March 2008; Volume 39.
48. Ramsley, K.R.; Head, J.W. The origin of Phobos grooves from ejecta launched from impact craters on Mars: Tests of the hypothesis. *Planet. Space Sci.* **2013**, *75*, 69–95. [CrossRef]
49. Murray, J.B.; Heggie, D.C. Character and origin of Phobos' grooves. *Planet. Space Sci.* **2014**, *102*, 119–143. [CrossRef]
50. Wilson, L.; Head, J.W. Groove formation on Phobos: Testing the Stickney ejecta emplacement model for a subset of the groove population. *Planet. Space Sci.* **2015**, *105*, 26–42. [CrossRef]
51. Ramsley, K.R.; Head, J.W. Origin of Phobos grooves: Testing the Stickney Crater ejecta model. *Planet. Space Sci.* **2019**, *165*, 137–147. [CrossRef]

52. Grier, J.A.; Rivkin, A.S. *Airless Bodies of the Inner Solar System: Understanding the Process Affecting Rocky, Airless Surfaces*, 1st ed.; Elsevier: Amsterdam, The Netherlands, 2019; pp. 229–253.

53. Shingareva, T.V.; Kuzmin, R.O. Mass-Wasting Processes on the Surface of Phobos. *Sol. Syst. Res.* **2001**, *35*, 431–443. [CrossRef]

54. Ramsley, K.R.; Head, J.W. The Stickney Crater ejecta secondary impact crater spike on Phobos: Implications for the age of Stickney and the surface of Phobos. *Planet. Space Sci.* **2017**, *138*, 7–24. [CrossRef]

55. Fernández, Y.R.; Li, J.-Y.; Howell, E.S.; Woodney, L.M. *Physics of Terrestrial Planets and Moons. Treatise on Geophysics*, 2nd ed.; Elsevier: Amsterdam, The Netherlands, 2015; pp. 487–527.

56. Thomas, P.C.; Veverka, J.; Sullivan, R.; Simonelli, P.; Malin, M.C.; Caplinger, M.; Hartmann, W.K.; James, P.B. Phobos: Regolith and ejecta blocks investigated with Mars Orbiter Camera images. *J. Geophys. Res.* **2000**, *105*, 15091–15106. [CrossRef]

57. Basilevsky, A.T.; Head, J.W.; Horz, F.; Ramsley, K. Survival times of meter-sized rock boulders on the surface of airless bodies. *Planet Space Sci* **2015**, *117*, 312–328. [CrossRef]

58. Ballouz, R.L.; Baresi, N.; Crites, S.T.; Kawakatsu, Y.; Fujimoto, M. Surface refreshing of Martian moon Phobos by orbital eccentricity-driven grain motion. *Nat. Geosci.* **2019**, *12*, 229–234. [CrossRef]

59. Popel, S.I.; Golub', A.P.; Zakharov, A.V.; Zelenyi, L.M. Dusty plasmas at Martian satellites. *J. Phys. Conf. Ser.* **2019**, *1147*, 012110. [CrossRef]

60. Miyamoto, H.; Niihara, T.; Wada, K.; Ogawa, K.; Senshu, H.; Michel, P.; Kikuchi, H.; Hemmi, R.; Nakamura, T.; Nakamura, A.M.; et al. Surface environment of Phobos and Phobos simulant UTPS. *Earth Planets Space* **2021**, *73*, 214. [CrossRef]

61. Lunine, J.I.; Neugebauer, G.; Jakosky, B.M. Infrared Observations of Phobos and Deimos from Viking. *J. Geophys. Res.* **1982**, *87*, 297–305. [CrossRef]

62. Kührt, E.; Giese, B.; Keller, H.U.; Ksanfomality, L.V. Interpretation of the Krfm-Infrared Measurements of Phobos. *Icarus* **1992**, *96*, 213–218. [CrossRef]

63. Sakatani, N.; Ogawa, K.; Iijima, Y.I.; Honda, R.; Tanaka, S. Experimental study for thermal conductivity structure of lunar surface regolith: Effect of compressional stress. *Icarus* **2012**, *221*, 1180–1182. [CrossRef]

64. Rosenblatt, P.; Lainey, V.; Le Maistre, S.; Marty, J.C.; Dehant, V.; Pätzold, M.; Van Hoolst, T.; Häusler, B. Accurate Mars Express orbits to improve the determination of the mass and ephemeris of the Martian moons. *Planet Space Sci* **2008**, *56*, 1043–1053. [CrossRef]

65. Lainey, V.; Dehant, V.; Pätzold, M. First numerical ephemerides of the Martian moons. *Astron. Astrophys.* **2007**, *465*, 1075–1084. [CrossRef]

66. Willner, K.; Oberst, J.; Hussmann, H.; Giese, B.; Hoffmann, H.; Matz, K.-D.; Roatsch, T.; Duxbury, T. Phobos control points network, rotation, and shape. *Earth Planet Sci. Lett.* **2010**, *294*, 541–546. [CrossRef]

67. Berthias, J. Analysis of the Phobos-2 Radiometric Data Set. *JPL Interoffice Memo.* **1990**, *314–316*, 1129.

68. Pätzold, M.; Andert, T.; Häusler, B.; Tellmann, S.; Tyler, G.L. Phobos mass determination from the very close Flyby of Mars Express in 2010. *Icarus* **2014**, *229*, 92–98. [CrossRef]

69. Yang, X.; Yan, J.G.; Andert, T.; Ye, M.; Pätzold, M.; Hahn, M.; Jin, W.T.; Li, F.; Barriot, J. The second-degree gravity coefficients of Phobos from two Mars Express flybys. *Mon. Not. R. Astron. Soc.* **2019**, *490*, 2007–2012. [CrossRef]

70. Konopliv, A.; Sjogren, W.L. *The JPL Mars Gravity Field Mars50c Based Upon Viking and Mariner-9 Doppler Tracking Data*; Jet Propulsion Laboratory: Pasadena, CA, USA, 1995.

71. Yuan, D.V.; Sjogren, W.L.; Konopliv, A.S.; Kucinskas, A.B. Gravity field of Mars: A 75th degree and order model. *J. Geophys. Res.* **2001**, *106*, 23377–23401. [CrossRef]

72. Konopliv, A.S.; Yoder, C.F.; Standish, E.M.; Yuan, D.-N.; Sjogren, W.L. A global solution for the Mars static and seasonal gravity, Mars orientation, Phobos and Deimos masses, and Mars ephemeris. *Icarus* **2006**, *182*, 23–50. [CrossRef]

73. Konopliv, A.S.; Asmar, S.W.; Folkner, W.M.; Karatekin, Ö.; Nunes, D.C.; Smrekar, S.E.; Yoder, C.F.; Zuber, M.T. Mars high resolution gravity fields from MRO, Mars seasonal gravity, and other dynamical parameters. *Icarus* **2011**, *211*, 401–428. [CrossRef]

74. The NIST Reference on Constants, Units, and Uncertainty. The 2018 CODATA Recommended Values of the Fundamental Physical Constants; Database developed by Baker, J., Douma, M., Kotochigova, S. Available online: http://physics.nist.gov/constants (accessed on 14 November 2022).

75. Busch, M.W.; Steven, J.; Ostro, S.J.; Lance, A.M.; Benner, L.A.M.; Giorgini, J.D.; Magri, C.; Howell, E.S.; Nolan, M.C.; Hine, A.A.; et al. Arecibo radar observations of Phobos and Deimos. *Icarus* **2007**, *186*, 581–584. [CrossRef]

76. Consolmagno, G.J.; Britt, D.T.; Macke, R.J. The significance of meteorite density and porosity. *Chem. Der. Erde* **2008**, *68*, 1–29. [CrossRef]

77. Carry, B. Density of asteroids. *Planet. Space Sci.* **2012**, *73*, 98–118. [CrossRef]

78. Hildebrand, A.R.; McCausland, P.J.A.; Brown, P.G.; Longstaffe, F.J.; Russell, S.D.J.; Tagliaferri, E.; Wacker, J.F.; Mazur, M.J. The fall and recovery of the Tagish Lake meteorite. *Meteorit. Planet. Sci.* **2006**, *41*, 407–431. [CrossRef]

79. Britt, D.T.; Consolmagno, G.J. Dark asteroids and dark meteorite densities (abstract). *Lunar Planet. Sci.* **1998**, *29*, 1577.

80. Macke, R.J.; Britt, D.T.; Consolmagno, G.J. Density, porosity, and magnetic susceptibility of achondritic meteorites. *Meteorit. Planet. Sci.* **2011**, *46*, 311–326. [CrossRef]

81. Richardson, D.C.; Leinhardt, Z.M.; Melosh, H.J.; Bottke, W.F.; Asphaug, E. Gravitational aggregates: Evidence and evolution. In *Asteroids III*, 1st ed.; Bottke, B., Cellino, A., Paolocchi, P., Binzel, R., Eds.; University of Arizona Press: Tucson, AZ, USA, 2002; pp. 501–515.